Molecular Communication System using Zn^{2+} Selective Supramolecular Nanochannel to induce Photoregulated Catalysis

Soumya Srimayee,[†a] Biswa Mohan Prusty,[†a] Mrinal Kanti Kar,[a] Mathias Winterhalter*[b,c], and Debasis Manna*[a]

[a.]Department of Chemistry, Indian Institute of Technology Guwahati, Guwahati, Assam, India.
[b.]Institute for Nanostructure and Solid-State Physics, University of Hamburg, Luruper Chaussee 149, 22761 Hamburg, Germany.
[c.]School of Science, Constructor University, Campus Ring 1, 28759 Bremen, Germany.

Email: dmanna@iitg.ac.in

1. General methods:

All chemical reactions were carried out in an inert atmosphere. Reagents and solvents for synthesis were purchased from commercial sources (Sigma Aldrich, TCI) and used without further purification. The column chromatography was performed using silica (100−200 mesh size). Thin-layer chromatography was carried out on silica gel 60-F254 plates. Egg yolk phosphatidylcholine (EYPC), mini extruder, and polycarbonate membranes of 100 nm and 200 nm were purchased from Avanti Polar Lipid. Magnesium green pentapotassium salt (MgG), Cholesterol, HEPES, lucigenin, Triton X-100, valinomycin, FCCP, CFDA-SE, DMSO, and all inorganic salts were obtained as molecular biology grade from Sigma Aldrich. The ^{1}H NMR spectra were recorded at 500 MHz, whereas the ^{13}C NMR spectra were recorded at 125 MHz. The residual solvent signals were considered as an internal reference (^{1}H NMR $CDCl_3$: δ_{ppm} 7.26 ppm; ^{13}C NMR $CDCl_3$: δ_{ppm} 77.2 ppm; ^{1}H NMR DMSO-d_6: δ_{ppm} 2.54 ppm; ^{13}C NMR DMSO-d_6: δ_{ppm} 39.5 ppm) to calibrate spectra. The chemical shifts were reported in parts per million (ppm). The following abbreviations were used to indicate multiplicity patterns: m: multiplet, s: singlet, d: doublet, t: triplet, q: quartet, dd: doublet of doublet, ddd: doublet of doublet of doublet, td: triplet of doublet, dt: doublet of triplet. Coupling constants were measured in Hz. High−resolution mass spectra (HRMS) were recorded on electrospray ionization time−of−flight (ESI−TOF). Fluorescence experiments were recorded using a Fluoromax-4 from HORIBA, equipped with an injector port and a magnetic stirrer in a microfluorescence cuvette. All buffer solutions were prepared from autoclaved water. The pH of buffer solutions was adjusted using the Helmer pH meter. The extravesicular dye was removed by performing gel chromatography using Sephadex G-50.

2. Synthesis and characterisation of compounds:

2.1. Synthesis of 1, 3, 5-triethyl-2, 4, 6-tris(isothiocyanatomethyl)benzene – To a stirring solution of 1,3,5-tris(bromomethyl)-2,4,6-triethylbenzene (**1**) (200 mg, 0.45 mmol) in dry DMF solvent, were added tetra butyl ammonium bromide (TBAB) (585 mg, 1.81 mmol), potassium thiocyanate (308 mg, 3.17 mmol) and sodium iodide (55 mg, 0.36 mmol) at room temperature under N_2 atmosphere. Then, the reaction mixture was stirred for 2-3 h at 80 °C. The progress of the reaction was monitored by TLC analysis. After

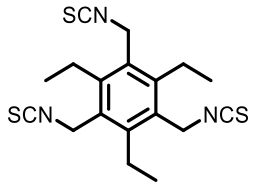

completion of the reaction, the unwanted salts were filtered through the filter paper. The filtrate was diluted with water (50 mL), and the organic layer was extracted with ethyl acetate (2 × 50 mL). The combined organic layers were dried over anhydrous sodium sulfate (Na2SO4) and concentrated under reduced pressure. The crude reaction mixture was purified through column chromatography using a solvent gradient system with ethyl acetate/hexane to yield a white solid compound with a 58% yield. The characterization of the compound matched the reported procedure.[1]

2.2. Synthesis of 2-phenyl-1*H*-benzo[d]imidazol-5-amine − Benzoyl chloride (1.44 g, 10.24 mmol) was added to a stirring solution of 4-nitrobenzene-1,2-diamine (1.54 g, 10.06 mmol) and Et_3N (1.5 mL, 10.76 mmol) in THF (100 mL) at 10 °C. The mixture was stirred overnight as it slowly warmed to room temperature. The mixture was diluted with water and extracted

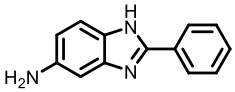

into ethyl acetate, and the product was recrystallized from acetonitrile as yellow crystals. To the obtained product (10 mmol), BF_3 etherate (1.5 mL, 12.92 mmol) was added, and the mixture was stirred in 1,4-dioxane (150 mL) and refluxed for 3 h. After cooling, the mixture was diluted with water and extracted with ethyl acetate. The product was purified on a column of silica gel eluting with hexanes/ethyl acetate (7:3), followed by recrystallization from ethyl acetate/hexanes as pale-yellow crystals (yield: 92%). Further, it was reduced catalytically over 0.5 g of 10% palladium-on-charcoal at normal pressure and room temperature to obtain the desired product (light yellow solid). Characterisation was matched according to the reported procedure.[2]

2.3. Synthesis of 2-(pyridin-2-yl)-1*H*-benzo[d]imidazol-5-amine − A mixture of an appropriate derivative of *o*-phenylenediamine, the corresponding carboxylic acid, and 5-20 equiv. of polyphosphoric acid was stirred in an oil bath at 180 °C for 2 h. The solution was

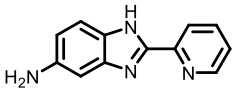

cooled and poured in a thin stream into rapidly stirred water. The pH was adjusted to 9 with sodium hydroxide. The solid was collected by filtration, dissolved in hot ethanol, and treated with charcoal. The ethanol was evaporated again, and the residue was recrystallized to obtain 2-Pyridin-2-yl-1*H*-benzimidazol, a white solid. To the solution of 2-pyridin-2-yl-1*H*-benzoimidazol in concentrated H_2SO_4, concentrated HNO_3 was added dropwise between 0 and 10 °C. The mixture was stirred at room temperature for 2 h and then poured into ice water.

Cautious neutralization with 50% NaOH provided a solid, which was filtered off and crystallized from MeOH to yield the desired product. 5-Nitro-2-pyridin-2-yl-1(3)*H*-benzimidazol as a light-yellow solid. 100 mg of nitro derivative was dissolved in 4 mL of absolute ethanol, and the solution was reduced catalytically over 0.5 g of 10% palladium-on-charcoal at normal pressure and room temperature. After the uptake of hydrogen was complete, the catalyst was removed by filtration, and the solvent was evaporated in vacuo. Upon recrystallization, the pure compounds were obtained. 2-Pyridin-2-yl-3H-benzoimidazol-5-ylamine as a light-yellow solid (yield: 78%). Characterisation was done according to the reported procedure.[3]

2.4. General procedure for synthesising tripodal compound 3a-3d − To the stirring solution of compound **1**, 3, 5-triethyl-2, 4, 6-tris(isothiocyanatomethyl)benzene (1.0 mmol) in DMF, different amines (3.0 mmol) were added and stirred overnight. The reactions were monitored through TLC. After the reaction was completed, ice-water was added, and the mixture was extracted with ethyl acetate (3 × 20 mL). The extract was then reduced under a rotary evaporator to obtain the crude solid. Column chromatography (hexane: ethyl acetate) was used to purify the product, and further characterization was performed on the same.

2.5.1. Synthesis of 1,1',1''-((2,4,6-triethylbenzene-1,3,5-triyl)tris(methylene))tris(3-phenylthiourea) (3a) − Compound **1** (0.1 mmol) and aniline (0.3 mmol) were used in the reaction following the general protocol mentioned above. The obtained crude solid was purified through column chromatography (hexane/ethyl acetate). Purified compound obtained as a pale-yellow solid in 60% yield.

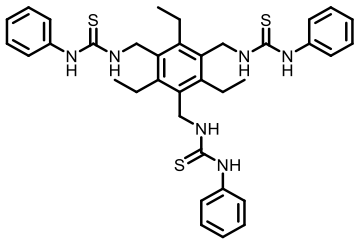

Characterisation: **^{1}H NMR** (400 MHz, DMSO-d_6) δ_{ppm}: 9.42 (s, 3H), 7.54 (d, J = 7.4 Hz, 8H), 7.31 (t, J = 7.9 Hz, 7H), 7.09 (t, J = 7.4 Hz, 3H), 4.73 (d, J = 4.0 Hz, 6H), 2.78 (q, J = 10.65 Hz, 6H), 1.18 (t, J = 7.34 Hz, 9H).**^{13}C NMR** (151 MHz, DMSO) δ_{ppm}: 180.56, 144.44, 140.06, 132.55, 128.90, 124.41, 123.04, 42.56, 23.32, 16.92. **HRMS**: ESI calc. for $C_{36}H_{42}N_6S_3$ $[M+H]^+$: 655.2706, found: 655.2706.

2.5.2. Synthesis of 1,1',1''-((2,4,6-triethylbenzene-1,3,5-triyl)tris(methylene))tris(3-(pyridin-2-yl)thiourea) (3b) −Compound **1** (0.1 mmol) and 2-aminopyridine (0.3 mmol) were used in the reaction following the general protocol mentioned above. The obtained crude solid was purified through column chromatography (hexane/ethyl acetate). Purified compound obtained as a white solid in 78% yield.

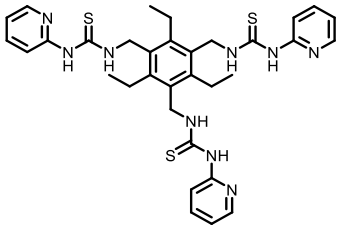

Characterisation: **^{1}H NMR** (600 MHz, DMSO-d_6) δ_{ppm}: 11.72 (t, J = 4.5 Hz, 3H), 10.69 (s, 3H), 7.72 (m, 3H), 7.59 (dd, J = 5.2, 1.9 Hz, 3H), 7.14 (d, J = 8.4 Hz, 3H), 6.79 (dd, J = 7.2, 5.1 Hz, 3H), 4.86 (d, J = 4.4 Hz, 6H), 2.83 (q, J = 7.5 Hz, 6H), 1.19 (t, J = 7.4 Hz, 9H). **^{13}C NMR** (151 MHz, DMSO) δ_{ppm}: 179.32, 154.20, 145.28, 144.31, 139.56, 132.51, 118.19, 113.14, 43.63, 23.11, 16.57. **HRMS**: ESI calc. for $C_{33}H_{39}N_9S_3$ $[M+H]^+$: 658.2563, found: 658.2567.

2.5.3. Synthesis of 1-(2-phenyl-1*H*-benzo[d]imidazol-5-yl)-3-(2,4,6-triethyl-3,5-bis((3-(2-phenyl-1*H*-benzo[d]imidazol-6-yl)thioureido)methyl)benzyl)thiourea (3c) −Compound **1** (0.1 mmol) and 2-phenyl-1*H*-benzo[d]imidazol-5-amine (0.3 mmol) were used in the reaction following the general protocol mentioned above. The crude solid was purified by column chromatography (hexane/ethyl acetate) to obtain a pale yellow solid in 54% yield.

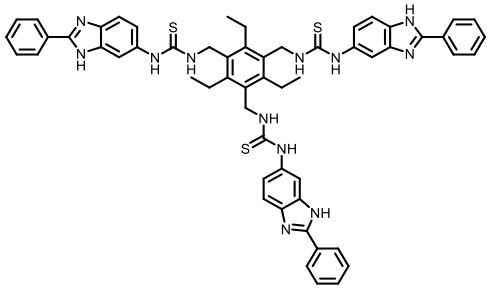

Characterisation: **^{1}H NMR** (600 MHz, DMSO-d_6) δ_{ppm}: 12.90 (s, 3H), 9.46 (s, 3H), 8.15 (d, J = 7.6 Hz, 5H), 8.11 (m, 1H), 7.82 (m, 2H), 7.65 – 7.43 (m, 13H), 7.12 (d, J = 97.9 Hz, 4H), 6.80 (d, J = 74 Hz, 1H), 4.98 (s, 2H), 4.74 (s, 4H), 2.80 (q, J = 12.96, 6H), 1.20 (t, J = 8.01 Hz, 9H). **^{13}C NMR** (151 MHz, DMSO) δ_{ppm}: 180.93, 152.10, 145.61, 144.10, 132.99, 130.47, 130.31, 129.61, 129.45, 128.24, 126.76, 42.72, 23.04, 16.59. **HRMS**: ESI calc. for $C_{57}H_{54}N_{12}S_3$ $[M+H]^+$: 1003.3829, found: 1003.3800.

2.5.4. Synthesis of 1-(2-(pyridin-2-yl)-1*H*-benzo[d]imidazol-5-yl)-3-(2,4,6-triethyl-3,5-bis((3-(2-(pyridin-2-yl)-1*H*-benzo[d]imidazol-6-yl)thioureido)methyl)benzyl)thiourea (3d) −Compound **1** (0.1 mmol) and 2-(pyridin-2-yl)-1*H*-benzo[d]imidazol-5-amine (0.3 mmol) were used in the reaction following general protocol mentioned above. The crude solid was purified through column chromatography (hexane/ethyl acetate) to obtain a pale-yellow solid in 54% yield.

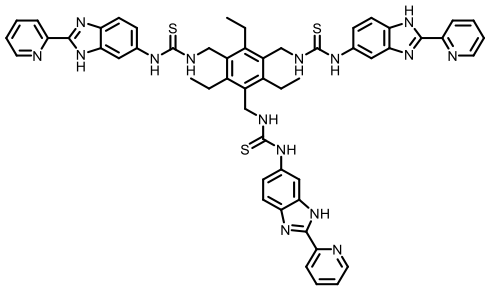

Characterisation: **^{1}H NMR** (400 MHz, DMSO-d_6) δ_{ppm}: 13.07 (d, J = 24.5 Hz, 3H), 9.49 (d, J = 23.7 Hz, 3H), 8.72 (d, J = 4.7 Hz, 3H), 8.29 (d, J = 7.5 Hz, 3H), 7.99 (t, J = 7.4 Hz, 3H), 7.89 (d, J = 16.6 Hz, 3H), 7.61 (d, J = 8.6 Hz, 2H), 7.55 – 7.44 (m, 7H), 7.22 (d, J = 8.7 Hz, 1H), 7.14 (d, J = 9.0 Hz, 2H),4.98 (s, 2H), 4.76 (s, 4H), 2.86 – 2.78 (m, 6H), 1.21 – 1.18 (m, 9H). **^{13}C NMR** (151 MHz, DMSO) δ_{ppm}: 180.98, 151.55, 149.85, 148.88, 145.62, 144.10, 137.99, 135.61, 132.99, 129.59, 128.28, 125.10, 121.76, 119.37, 107.02, 42.76, 23.04, 16.59. **HRMS**: ESI calc. for $C_{54}H_{51}N_{15}S_3$ $[M+H]^+$: 1006.3687, found: 1006.3628.

2.5.5 Synthesis of 1-(3-((3-(2-(pyridin-2-yl)-1*H*-benzo[d]imidazol-5-yl)thioureido)methyl) benzyl)-3-(2-(pyridin-2-yl)-1*H*-benzo[d]imidazol-6-yl) thiourea (5a) − To the stirring solution of 1,3-bis(isothiocyanatomethyl)benzene (0.5 mmol) in dry DMF 2-(pyridin-2-yl)-1*H*-benzo[d]imidazol-5-amine (1 mmol) was added dropwise and stirred for overnight. The reaction was monitored by TLC until it was complete. Afterwards, the compound was extracted with ethyl acetate (20 mL × 3) and reduced under pressure. The resulting solid was purified through column chromatography (ethyl acetate/hexane). A pale yellow solid was obtained in moderate yield (58%).

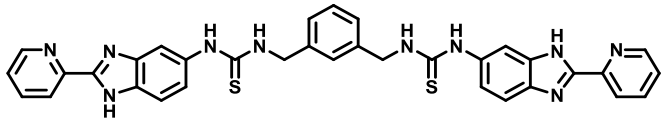

Characterisation: **^{1}H NMR** (600 MHz, DMSO-d_6) δ_{ppm}: 13.12 (d, J = 34.8 Hz, 2H), 9.70 (d, J = 35.5 Hz, 2H), 8.73 (s, 2H), 8.31 (d, J = 6.8 Hz, 2H), 8.13 (s, 1H), 8.04 (s, 1H), 7.99 (t, J = 7.8 Hz, 2H), 7.69 (s, 1H), 7.66 (d, J = 6.8 Hz, 2H), 7.52 (d, J = 7.9 Hz, 3H), 7.33 (t, J = 6.87 Hz, 1H), 7.29 (s, 1H), 7.24 (d, J = 6.7 Hz, 2H), 7.19 (d, J = 8.3 Hz, 1H), 7.15 (d, J = 8.7 Hz, 1H), 4.76 (s, 4H). **^{13}C NMR** (151 MHz, DMSO) δ_{ppm}: 181.43, 151.94, 151.60, 149.88, 148.82,

144.41, 141.97, 139.75, 138.04, 135.41, 133.29, 128.66, 126.67, 126.25, 125.15, 121.76, 119.75, 112.54, 108.32, 47.82. **HRMS**: ESI calc. for $C_{34}H_{28}N_{10}S_2$ $[M+H]^+$: 641.2013, found: 641.1979.

2.6 Lipophilicity of the synthesized compounds — To clarify the structure–function relationship and address the role of lipophilicity, we calculated membrane partition coefficient (clogP) values for all the synthesized compounds using ChemDraw (R-25.5) software. The tripodal compound shows a clogP of 9.96, while the dipodal receptor shows a clogP of 5.39. Although the tripodal system is more lipophilic, both values exceed the clogP value of 5, indicating a strong membrane affinity; therefore, differences in partitioning alone cannot account for the substantial variation in ion transport activity. It was reported that a compound with reduced mobility and channel/pore-forming properties, acting as a signal transducer, requires higher logP values to ensure good membrane confinement.[4] Hence, we can conclude that the lipophilic nature of the tripodal entity is an additional factor contributing to its higher transport efficacy compared to its dipodal counterpart.

Table S1. Calculated membrane partition coefficient (clogP) values using ChemDraw (R-25.5) software.

Compound	clogP
3a	6.59
3b	5.02
3c	13.34
3d	9.96
5a	5.39

3. Transport experiments:

3.1. Preparation of EYPC/Chol-LUV⊃MgG vesicles — To conduct the MgG fluorescence-based ion-transport studies, we took EYPC (50 mg/mL in deacidified $CHCl_3$) and cholesterol (CHOL; 25 mg/mL in deacidified $CHCl_3$) in a clean, dry glass vial in a molar ratio of 8:2. The solution was evaporated for 6 h under reduced pressure to form a thin lipid film. After that, we rehydrated the film with 10 mM HEPES buffer containing 100 mM NaCl, 100 μM EDTA, and 50 μM MgG dye at pH 7.0. The resulting suspension was vortexed six to seven times over a 1 h period. Next, we performed 6-7 freeze-thaw cycles followed by 10 minutes of constant vortexing. We then extruded the lipid suspension 19–21 times using a mini extruder with a 200 nm pore size to achieve a uniform liposome size of 200 nm. Finally, we removed the

unencapsulated MgG dye using the gel filtration technique (Sephadex G-50) and 10 mM HEPES buffer containing 100 mM NaCl at pH 7.0 as the eluting solution. This process yielded a final lipid concentration of 25 mM (assuming 100% lipid regeneration).[5]

3.2. Transport assays with EYPC/Chol-LUV⊃MgG vesicles — For the MgG-based ion transport assay, in a clean and dry fluorescence cuvette (3 mL), 10 mM HEPES buffer containing 100 mM NaCl, pH 7.0 (1930 µL), EYPC/Chol-LUV⊃MgG (40 µL), and $ZnCl_2$ (final concentration 1 mM) were added. The cuvette was placed under slow stirring conditions in a fluorescence spectrophotometer for about 3 minutes to equilibrate. The fluorescence was evaluated as a function of time (λ_{em} = 531 nm, λ_{ex} = 506 nm). At 50 s, 10 µL of compound was added to the cuvette solution to initiate the transport studies. Finally, the vesicles were completely lysed at 450 s by adding 20 µL of 20% Triton X-100. Transport studies for the compounds were performed in triplicate at various concentrations of compound **3d** (5 nM to 200 nM). The fluorescence intensity measurement was continued for a further 50 s. The normalized % transport efficiency (%EE) at t = 450 s was considered for the particular transport efficiency of the compounds.

Transport activity, $T_{MgG} = (\frac{F_t - F_0}{F_\infty - F_0} \times 100)$ %

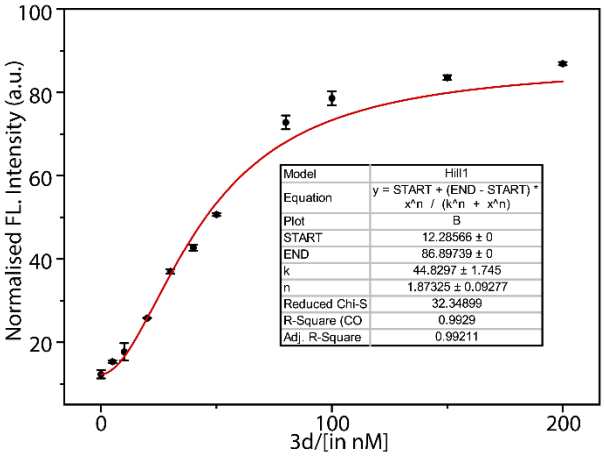

Fig. S1. Concentration-dependent transmembrane Zn^{2+} transport efficacy of compound **3d** across EYPC/Chol-LUV⊃MgG. The EC_{50} value was calculated using the Hill 1 equation.

3.3. Critical aggregation concentration measurements — The critical aggregation concentration (CAC) of compound **3d** was determined using its concentration-dependent Zn^{2+} transport properties. A distinct inflection point was observed through the linear fitting after analysing the % transport (Zn^{2+}) in the lower concentration range. Below 15 nM, the slope of the linear fit was 0.58 ± 0.05, while above 15 nM, the slope increased to 0.92 ± 0.09. The change in slope at the inflection point suggests the initiation of supramolecular nanochannels

(> 15 nM) under liposomal conditions. The final concentration of LUVs was 0.5 mM during this measurement.

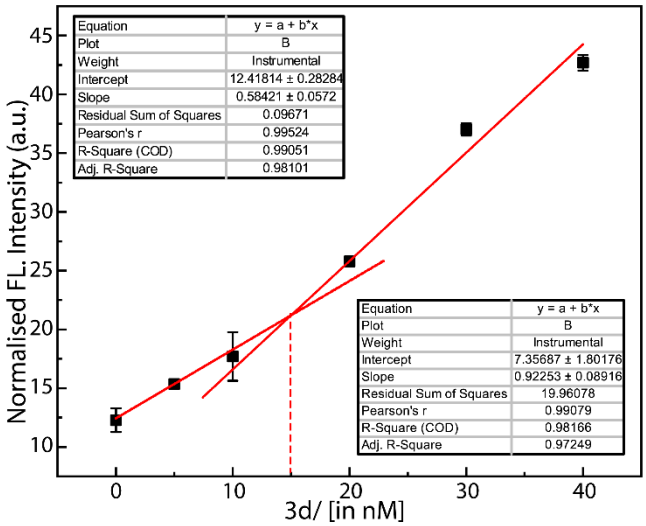

Fig. S2. Measurement of CAC values of compound **3d** calculated from the concentration-dependent Zn^{2+} ions transport properties across EYPC/Chol-LUV⊃MgG.

Note: The critical aggregation constant (CAC) value, determined from concentration-dependent ion transport studies of compound **3d**, was approximately 15 nM (Fig. S2), which indicates that supramolecular channels of compound **3d** begin to form within the vesicles at concentrations greater than 15 nM.

3.4. Cation selectivity studies across EYPC/Chol-LUV⊃MgG vesicles — For the cation selectivity studies, a similar procedure was followed for preparing vesicles and measuring ion transport activities, as mentioned in the previous section. For the fluorescence assay, 10 mM HEPES buffer containing 100 mM NaCl, pH 7.0 (1930 µL), EYPC/Chol-LUV⊃MgG (40 µL), and M_xCl_y salt (1 mM final conc.) ($MgCl_2$, $MnCl_2$, $FeCl_3$, $CoCl_2$, $NiCl_2$, $CuCl_2$, $ZnCl_2$) were taken in a clean fluorescence cuvette (3 mL). The cuvette was placed in the spectrofluorometer under slow stirring conditions for approximately 3 minutes. The MgG fluorescence intensity was recorded as a function of time (λ_{em} = 531 nm, λ_{ex} = 506 nm). At 50 s, 10 µL of compound **3d** was added to the cuvette solution (final concentration, 50 nM), initiating the transport studies. Finally, the vesicles were lysed entirely by adding 20 µL of 20% Triton X-100 at 450 s, and the fluorescence intensity measurement was continued for a further 50 s. The studies on cation selectivity were conducted multiple times.

[Note: Further transport of monovalent ions like Na^+ and K^+ was conducted in EYPC/Chol-LUV⊃HPTS. This demonstrated that the compound **3d** has negligible transport efficacy for monovalent ions.

Cation Selectivity studies across EYPC/CHOL-LUV⊃HPTS — The cation selectivity studies were performed according to the reported procedure. Briefly, in a clean fluorescence cuvette, 1940 µL of buffer solution (100 mM MCl, 20 mM HEPES, pH 7.2; where M^+ = Na^+, K^+), 50 µL of EYPC/CHOL-LUV⊃HPTS (prepared in 20 mM HEPES buffer containing 100 mM NaCl, pH 7.2) and fluorescence cuvette was placed in a fluorescence instrument equipped with a magnetic stirrer at t = 0 s. The fluorescence emission intensity of the HPTS dye was measured at λ_{em} = 510 nm (where λ_{ex} = 450 nm) for the time course of 0 to 500 s. At t = 50 s, compound **3d** was introduced between the intra- and extravesicular media, initiating the kinetics study. Triton X-100 (20 µL of 20% solution in water) was added at t = 450 s to destroy all the vesicles.

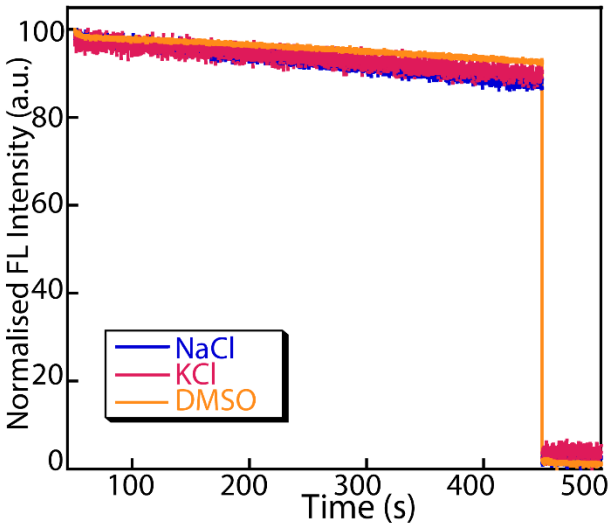

Fig. S3. Cation selectivity study for compound **3d** across EYPC/CHOL-LUVs⊃HPTS, where intravesicular solution contains 20 mM HEPES buffers containing 100 mM NaCl, HPTS (1 mM) at pH 7.2, and extravesicular solution contains 20 mM HEPES buffers, 100 mM MCl (where M^+ = Na^+, K^+) at pH = 7.2.]

3.4. Anion selectivity studies across EYPC/Chol-LUV⊃MgG vesicles — For the anion selectivity studies, a similar procedure was followed for preparing vesicles and measuring ion transport activities, as mentioned in the previous section. For the fluorescence assay, 10 mM HEPES buffer containing 100 mM NaCl, pH 7.0 (1930 µL), EYPC/Chol-LUV⊃MgG (40 µL), and Zn_xB_y (1 mM final concentration of $ZnCl_2$, $ZnBr_2$, $ZnSO_4$, and $Zn(NO_3)_2$) were taken in a clean fluorescence cuvette (3 mL). The cuvette was placed in a spectrofluorometer under slow

stirring conditions for approximately 3 minutes. The MgG fluorescence intensity was monitored as a function of time (λ_{em} = 531 nm, λ_{ex} = 506 nm). At 50 s, 10 μL of compound **3d** (final conc. 50 nM) was added to the cuvette solution to initiate the transport studies. Finally, the vesicles were lysed by adding 20 μL of 20% Triton X-100 for 450 s, and the fluorescence intensity measurement was continued for a further 50 s. The studies on anion selectivity were conducted multiple times.

3.5. Investigation of Cl^- ion transport ability of the compound across the EYPC/Chol-LUVs⊃lucigenin — To study ion transport using lucigenin fluorescence, large unilamellar vesicles (LUVs) composed of egg yolk phosphatidylcholine (EYPC) and cholesterol (CHOL) were prepared. EYPC (50 mg/mL in deacidified $CHCl_3$) and CHOL (25 mg/mL in deacidified $CHCl_3$) were mixed in a clean glass vial in an 8:2 molar ratio. The organic solvent was evaporated under reduced pressure for 6 h, resulting in a uniform, thin lipid film. The lipid film was hydrated by adding 800 μL of 20 mM HEPES buffer containing 1 mM lucigenin and 100 mM $NaNO_3$ (pH 7.0). The resulting suspension was subjected to six to seven vortex cycles over 1 h to ensure homogeneity, followed by 17–19 freeze-thaw cycles. Subsequently, the suspension underwent constant vortexing for 10 minutes to encapsulate lucigenin within the lipid bilayer. Using a mini extruder, the lipid suspension was extruded through a 200 nm polycarbonate membrane (Avanti Polar Lipids). This extrusion process was repeated 19–21 times (ensuring an odd number of passes) to obtain uniformly sized LUVs. Unencapsulated lucigenin dye was removed by size-exclusion chromatography using a Sephadex G-50 column equilibrated with 20 mM HEPES buffer containing 100 mM $ZnCl_2$ (pH 7.0) to get the final lipid concentration of 25 mM (assuming 100% lipid regeneration). For the fluorescence-based transport assay, 1940 μL of 20 mM HEPES buffer containing 100 mM $ZnCl_2$ (pH 7.0) and 50 μL of the EYPC/CHOL-LUV⊃lucigenin LUV suspension were transferred to a quartz fluorescence cuvette. The sample was maintained at room temperature under slow stirring. Fluorescence emission was monitored using a spectrophotometer at an excitation wavelength of 455 nm and an emission wavelength of 505 nm. After recording the baseline fluorescence for 50 seconds, 10 μL of compound **3d** (from a DMSO stock solution) was added to initiate ion transport. At 450 seconds, the vesicles were lysed by adding 20 μL of 20% Triton X-100 solution, and fluorescence was recorded until 500 seconds to determine the endpoint.

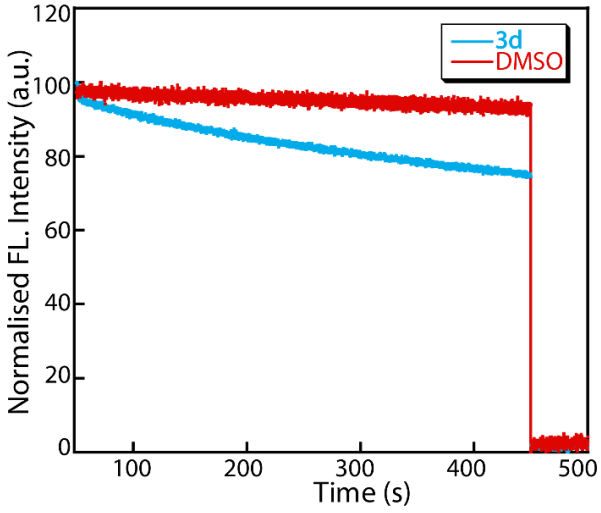

Fig. S4. Chloride ion transport activity of compound **3d** (10 μM) across EYPC/Chol-LUV⊃lucigenin, with DMSO (10 μL) as the control.

3.6. Binding affinity of 3d with Zn^{2+} — The binding affinity of compound **3d** for Zn^{2+} was examined through UV-Vis titration of the water medium. In this experiment, a 10 μM solution of compound **3d** was titrated with $ZnCl_2$, resulting in a gradual decrease in absorbance with each addition of Zn^{2+} ions. The association constant (K_a) for the interaction was determined using the Bindfit v0.5 program by fitting the absorbance data to a 1:1 binding model. Under the experimental conditions, the calculated (average of three measurements) K_a was 7438.92 ± 2.7 M^{-1}.

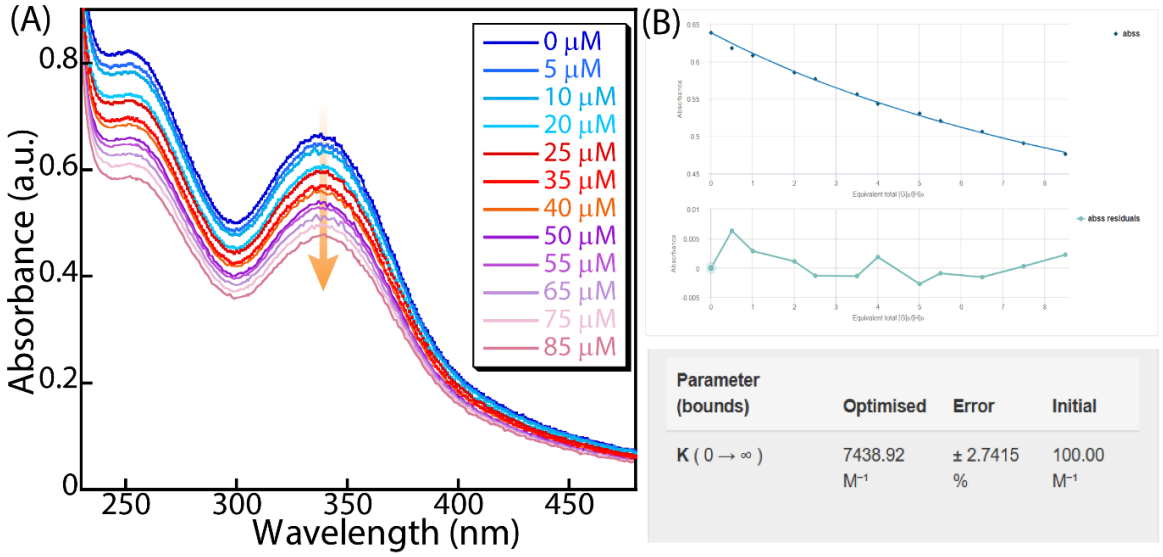

Fig. S5. Representative UV-Vis absorbance titration spectra of compound **3d** (10 μM) with varying concentrations of Zn^{2+} ions (0-85 μM). (B) Calculation of binding constant using the BindFit 0.5 program.

Note: The ^{1}H NMR-based interaction of compound **3d** (10 mM) with Zn^{2+} (40 µM) was measured in DMSO-d_6, which clearly showed that the benzimidazole NH proton showed a strong interaction with the Zn^{2+}, which causes a proton shift from 13.1 to 14.5 ppm (Fig. S14), concluding the de-shielding effect imparted by the Zn^{2+}. Whereas, in Figure. S15 the partial drift of thiourea NH from 9.43 to 9.59 suggests that Zn^{2+} weakly interacts with the thiourea group (S atom of the thiourea group), which causes a partial de-shielding effect in the proton.

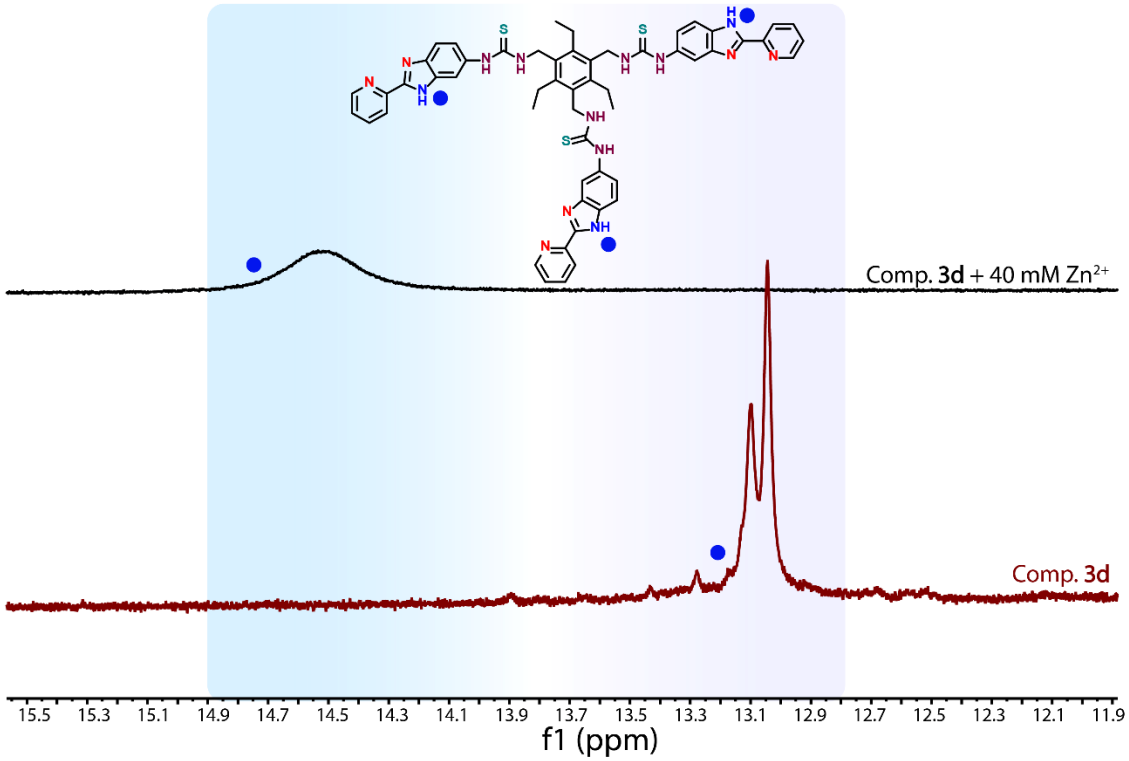

Figure. S6. Stacked image (^{1}H NMR) of the interaction between the benzimidazole NH of compound **3d** with 40 µM Zn^{2+}.

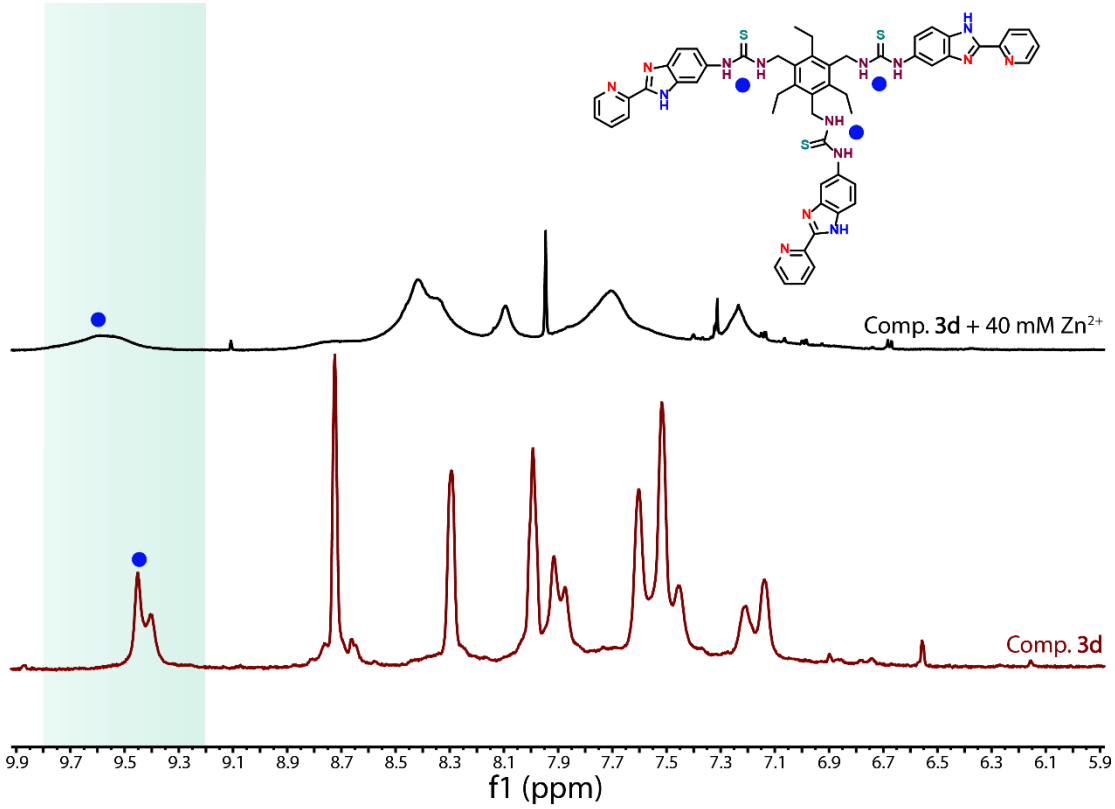

Figure. S7. Stacked image (^{1}H NMR) of the interaction between the thiourea NH of compound **3d** with 40 μM Zn^{2+}.

Note: Although receptor **3d** exhibits a moderate Zn^{2+} binding constant in aqueous media (K_a = 7439 ± 3 M^{-1}), this affinity actually places the system within the "Goldilocks" binding regime required for efficient ion transport. Transmembrane ion transport requires reversible binding; very weak affinity would lead to poor ion recognition, while excessively strong binding could hinder ion release and potentially block the channel. Literature reports repeatedly highlight that optimal, rather than maximal, binding affinity is essential for efficient ion translocation.[4, 6, 7]

The binding affinity was measured in aqueous media, whereas the ion transport studies were performed using model lipid bilayers. The receptor may behave differently in bulk solution versus within the lipid bilayer.

Within the lipid bilayers:

• Competition from water is significantly reduced, which could strengthen ion-ligand interactions.

• Hydrophobic partitioning increases the local receptor concentration.

• Restricted mobility enhances the preorganization of the binding motifs.

• Membrane-induced self-assembly creates channel-like architectures that could cooperatively facilitate ion capture and release.

Therefore, even moderate affinity in solution may lead to stronger and more effective coordination under transport conditions. Additionally, because compound **3d** functions as a channel-forming assembly rather than a mobile carrier, only moderate affinity is needed to efficiently shuttle ions across the bilayer without creating a transport barrier.

3.7. Ion transport study across EYPC/Chol-LUV⊃MgG in the presence of FCCP — For the FCCP assay, the vesicles were prepared similarly as mentioned in the earlier section using 10 mM HEPES, 100 mM NaCl, 100 µM EDTA buffer pH 7.0. In a clean fluorescence cuvette (3 mL), 10 mM HEPES buffer containing 100 mM NaCl, pH 7.0 (1930 µL), EYPC/Chol-LUV⊃MgG (40 µL), Zn^{2+} (final concentration 1 mM), and FCCP (1.0 nM) were taken. The cuvette was placed in the spectrofluorometer under slow stirring conditions for approximately 3 minutes. The fluorescence intensity was recorded as a function of time (λ_{em} = 531 nm, λ_{ex} = 506 nm). At 50 s, 10 µL of compound **3d** was added to the cuvette solution (final concentration, 50 nM), initiating the transport studies. Finally, the vesicles were lysed entirely by adding 20 µL of 20% Triton X-100 at 450 s, and the fluorescence intensity measurement continued for a further 50 s. The control experiment was performed in the presence of DMSO and only FCCP. The FCCP assay was performed in multiple.

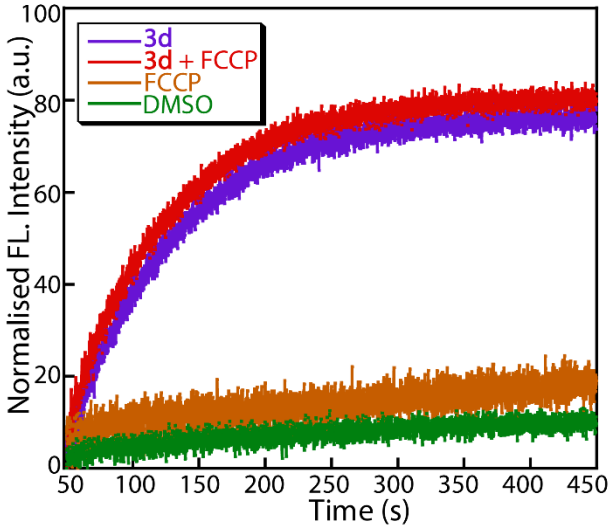

Fig. S8. Ion transport activity of compound **3d** (50 nM) in the absence and presence of FCCP (1 nm) across EYPC/CHOL-LUV⊃MgG. The vesicles were prepared in 10 mM HEPES buffer containing 100 mM NaCl and 100 µM EDTA, pH 7.0, and suspended in 10 mM HEPES buffer containing 100 mM NaCl and 100 µM EDTA, pH 7.0. DMSO (10 µL) was used as a control.

3.8. Fluorescein-based assay to monitor pH modulation along with Zn^{2+} transportation across EYPC/CHOL-LUVs⊃fluorescein vesicles — To conduct the fluorescein-based ion

transport measurements for monitoring pH changes along with Zn^{2+} ion transport process within the vesicles, LUVs were prepared similarly as mentioned in the earlier section using 10 mM fluorescein dye in 10 mM HEPES buffer containing 100 mM NaCl at pH 6.0. In a clean fluorescence cuvette (3 mL), 10 mM HEPES buffer containing 100 mM NaCl, pH 6.0 (1930 µL), EYPC/Chol-LUV⊃fluorescein (40 µL), and $ZnCl_2$ (final concentration 3 mM) were added. The cuvette was placed under slow stirring conditions in a fluorescence spectrophotometer for about 3 minutes to equilibrate. The fluorescence was evaluated as a function of time (λ_{em} = 520 nm, λ_{ex} = 495 nm). At 50 s, compound **3d** (1 µM) was added to the cuvette solution to initiate the transport studies. Similarly, transport studies were also performed using various extravesicular buffers of different pH levels (pH 6.5 and 7.0). The normalized fluorescence intensity was determined by using the equation below,

$$I_{rel} = \frac{I_t}{I_{min}}$$

where I_t is the fluorescence intensity at time t, and I_{min} is the fluorescence minima of the particular kinetics.

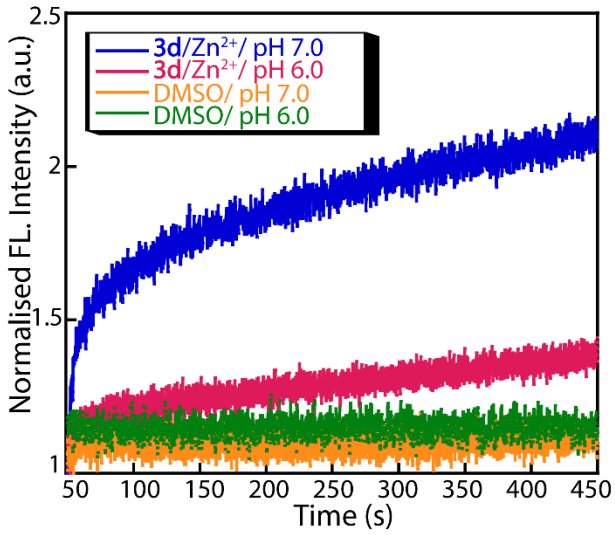

Fig. S9. Measurement of intravesicular pH modulation upon addition of compound **3d** across EYPC/Chol-LUV⊃fluorescein suspended in 10 mM HEPES buffer containing 100 mM NaCl at pH 6.0/7.0 after the addition of 3 mM $ZnCl_2$ and 1 µM compound **3d** in the extravesicular environment. The intravesicular solution was 10 mM HEPES buffer containing 100 mM NaCl at pH 6.0.

3.9. Ion transport study across EYPC/Chol-LUV⊃MgG in the presence of valinomycin — For the valinomycin assay, the liposomes were prepared similarly as mentioned in the earlier section using 10 mM HEPES, 100 mM KCl, 100 µM EDTA, pH 7.0. In a clean fluorescence cuvette (3 mL), 10 mM HEPES buffer containing 100 mM NaCl, pH 7.0 (1930 µL),

EYPC/Chol-LUV⊃MgG (40 µL), Zn^{2+} (final concentration 1 mM), and valinomycin (12 pM) was taken. The cuvette was placed in the spectrofluorometer under slow stirring conditions for approximately 3 minutes. The fluorescence intensity was recorded as a function of time (λ_{em} = 531 nm, λ_{ex} = 506 nm). At 50 s, 10 µL of compound **3d** was added to the cuvette solution (final concentration 50 nM), which initiated the transport studies. Finally, the vesicles were lysed entirely by adding 20 µL of 20% Triton X-100 at 450 s, and the fluorescence intensity measurement continued for a further 50 s. The control experiment was performed in the presence of DMSO and only valinomycin. The valinomycin assay was performed in multiple.

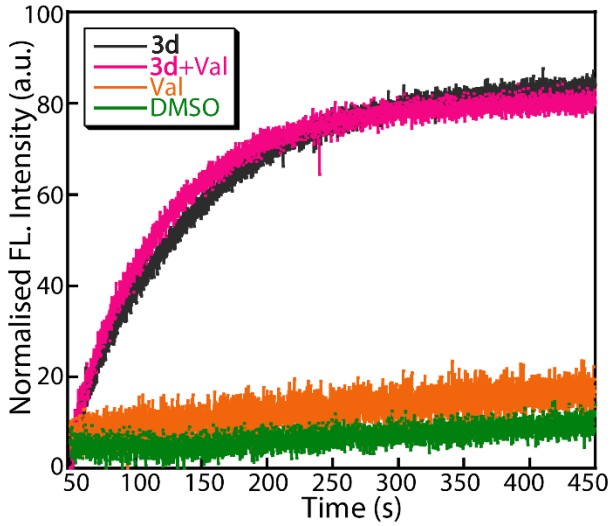

Fig. S10. Ion transport activity of compound **3d** (50 nM) in the absence and presence of valinomycin (12 pM) across EYPC/CHOL-LUV⊃MgG. The vesicles were prepared in 10 mM HEPES buffer containing 100 mM KCl and 100 µM EDTA, pH 7.0, and suspended in 10 mM HEPES buffer containing 100 mM NaCl and 100 µM EDTA, pH 7.0. Val = valinomycin. DMSO (10 µL) was used as a control.

3.10. Vesicle leakage assay across EYPC−LUV⊃carboxyfluorescein — A thin lipid film was prepared by evaporating a solution of 154 µL of EYPC (50 mg/mL stock in chloroform), and 39 µL cholesterol (25 mg/mL stock in chloroform) in vacuo for 6 h.[8] After that, the lipid film was hydrated with 500 µL buffer (10 mM HEPES, 10 mM $NaNO_3$, 50 mM carboxyfluorescein (CF), pH 7.0) for 1 h with occasional vortexing of 4−5 times and then subjected to freeze-thaw cycle (≥ 15 times). The vesicle solution was extruded through a polycarbonate membrane with 200 nm pores 19 times (an odd number) to yield vesicles with a mean diameter of ~ 200 nm. The extracellular dye was removed using size exclusion chromatography (Sephadex G-50) with 10 mM HEPES buffer (100 mM NaCl, pH 7.0). Final

concentration: ~25 mM EYPC-CHOL lipid; intravesicular solution: 10 mM HEPES, 10 mM $NaNO_3$, 50 mM CF, pH 7.0; extravesicular solution: 10 mM HEPES, 100 mM NaCl, pH 7.0.

3.11. Carboxyfluorescein leakage assay — In a clean and dry fluorescence cuvette, 50 µL of the above lipid solution and 1930 µL of 10 mM HEPES buffer, 100 mM NaCl, pH 7.0, were taken and kept in a slowly stirring condition by a magnetic stirrer equipped with the fluorescence instrument (at t = 0 s). The CF fluorescence emission intensity time course, F_t, was observed at λ_{em} = 517 nm (λ_{ex} = 492 nm). Compound **3d** was added at t = 50 s, and at t = 450 s, 20 µL of 20% Triton X-100 was added to lyse those vesicles for 100% CF release. This study confirmed that the integrity of the bilayer membranes is intact in the presence of varying concentrations of compound **3d**.

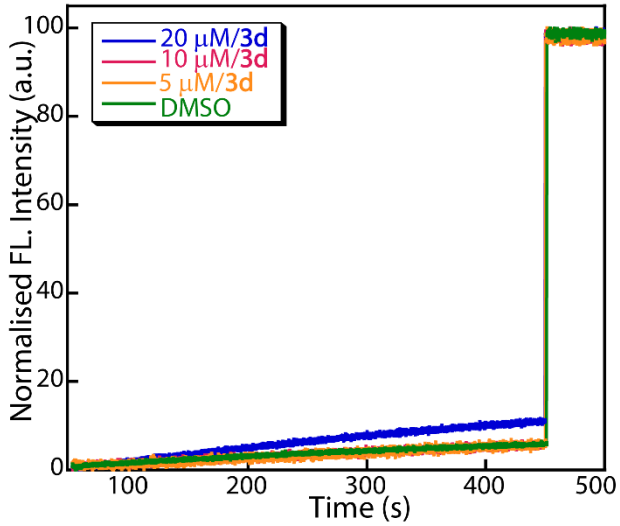

Fig. S11. Vesicle leakage assay of compound **3d** using EYPC/Chol-LUV⊃CF. DMSO (10 µL) was used as a control.

3.12. Ion transport study across EYPC/Chol-LUV⊃MgG vesicles for cholesterol dependency assay — To get an insight into channel or carrier-like behaviour of the potent compound, the cholesterol dependency assay was performed across EYPC/Chol-LUV⊃MgG. The vesicles were prepared according to the earlier-mentioned procedure with varying percentages of cholesterol. The LUVs with 8:2 and 6:4 molar ratios of EYPC/Chol were prepared, encapsulating 10 mM HEPES buffer containing 100 mM NaCl, 100 µM EDTA at pH 7.0, and 50 µM MgG. In a clean fluorescence cuvette (3 mL), 10 mM HEPES buffer containing 100 mM NaCl, pH 7.0 (1930 µL), EYPC/Chol-LUV⊃MgG (40 µL) of 8:2 ratio, and Zn^{2+} (final concentration 1 mM) were taken. The cuvette was placed in the spectrofluorometer under slow stirring conditions for approximately 3 minutes. The fluorescence intensity was recorded as a

function of time (λ_{em} = 531 nm, λ_{ex} = 506 nm). At 50 s, 10 µL of compound **3d** was added to the cuvette solution (final concentration, 50 nM), which initiated the transport studies. Finally, the vesicles were lysed entirely by adding 20 µL of 20% Triton X-100 at 450 s, and the fluorescence intensity measurement continued for a further 50 s. The same procedure was followed for measuring transport across EYPC/Chol-LUVs with a 6:4 ratio. DMSO control (10 µL) was measured with both 8:2 and 6:4 ratio-based vesicles. [9]

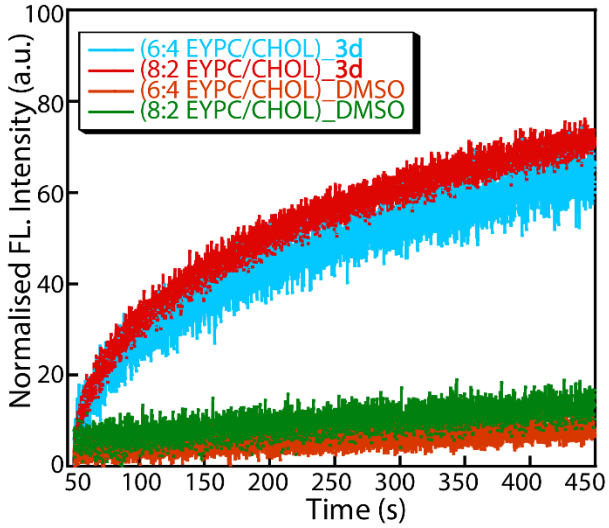

Fig. S12. Cholesterol concentration-dependent Zn^{2+} transport activity of compound **3d** (50 nM) using EYPC/Chol-LUV⊃MgG with a molar ratio of 8:2 and 6:4 (EYPC/Chol). The vesicles were prepared using 10 mM HEPES buffer containing 100 mM NaCl, 100 µM EDTA, and MgG dye at pH 7.0, and suspended in 10 mM HEPES buffer containing 100 mM NaCl and 100 µM EDTA at pH 7.0. DMSO (10 µL) was used as a control.

3.13. U-Tube assay for compound 3d – The classical U-tube experiment was performed to confirm the mechanistic pathway for the Zn^{2+} ion transport by compound **3d**. The lipid bilayer was mimicked using chloroform (12 mL) as the organic layer. The compound **3d** (2 mM) in chloroform was placed at the bottom of the U-tube under mild stirring conditions. The left arm of the tube was filled with 20 mM HEPES and $ZnCl_2$ solution (12 mL, 0.1 M), and the right arm was filled with 20 mM HEPES and 0.1 M aqueous $NaNO_3$ solution (12 mL). Arsenazo-III, a metal ion-sensing dye (20 µM), was added to the receiver arm for sensing Zn^{2+}. The Zn^{2+} ion binding to arsenazo-III dye (20 µM; λ_{max} = 545 nm) showed a significant shift in UV-Vis spectra (λ_{max} = 600 nm). The Zn^{2+} concentration at the receiver end was monitored using a UV-Vis spectrophotometer after 72 h. The obtained spectra suggested that after 72 h, no significant amount of Zn^{2+} was carried to the receiver end of the U-tube. Hence, compound **3d** could not

act as a carrier through an apolar phase ($CHCl_3$). A similar study was performed in the presence of clioquinol (CQ, 2 mM), a Zn^{2+} carrier.

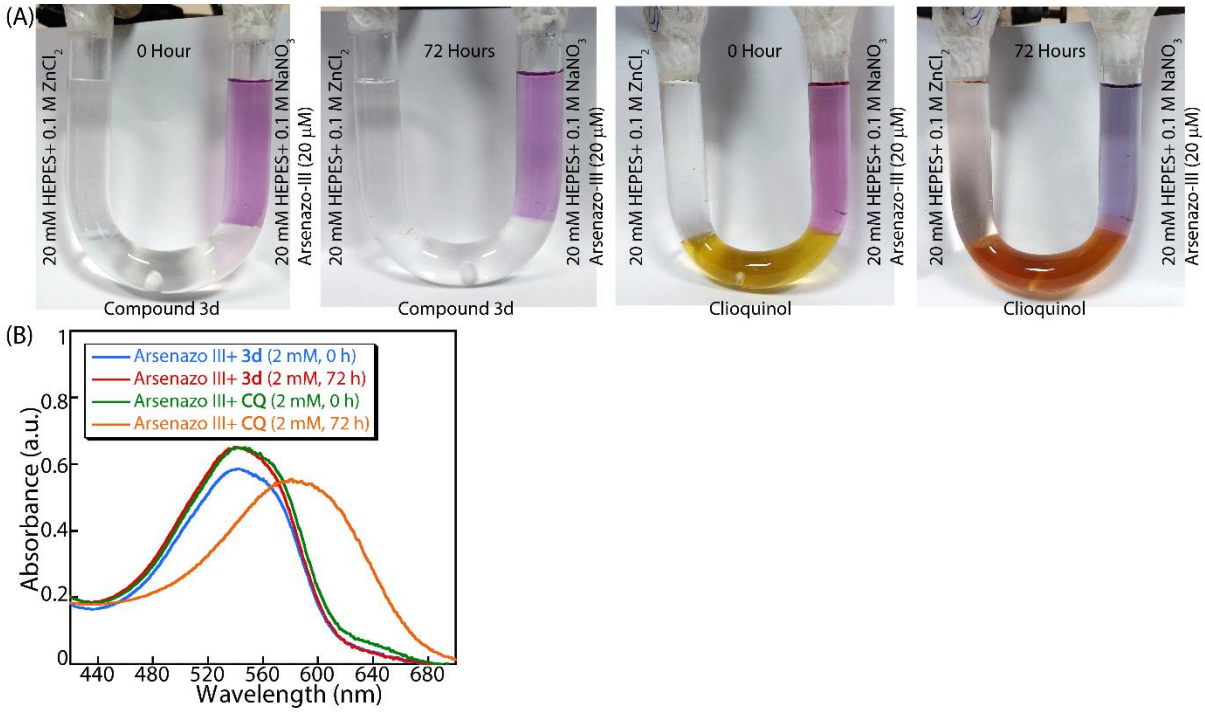

Fig. S13. (A) U-tube assay of compound **3d** and clioquinol (CQ; control). (B) UV-Vis absorbance spectra of arsenazo-III dye-containing solution from the receiver end of the U-tube in the presence of compound **3d** and CQ at 0 and 72 h.

4. Field emission scanning electron microscopy (FESEM) analysis:

To understand the effect of solvent polarity on the self-assembly properties of the compound, we conducted a morphological study using FESEM analysis. Compound **3d** (1 mM) solutions in water and $CHCl_3$ were prepared and then drop-casted for the FESEM experiment and dried at room temperature. Before analysis, the samples were stacked onto the FESEM grid and coated with a gold solution.[10]

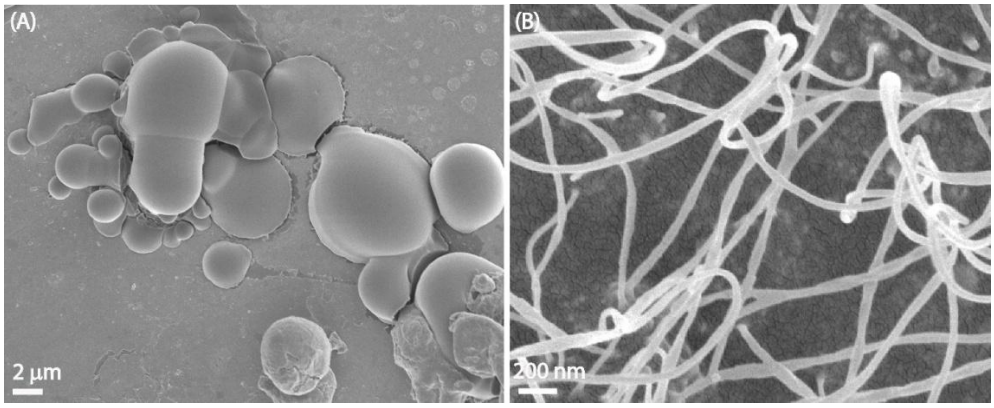

Fig. S14. Morphological analysis using FESEM of compound **3d** in (A) hydrophilic (H_2O) and (B) hydrophobic ($CHCl_3$) environment.

5. NOESY spectra of the compound:

The NOESY spectrum of compound **3d** was recorded in DMSO-d_6 solvent.

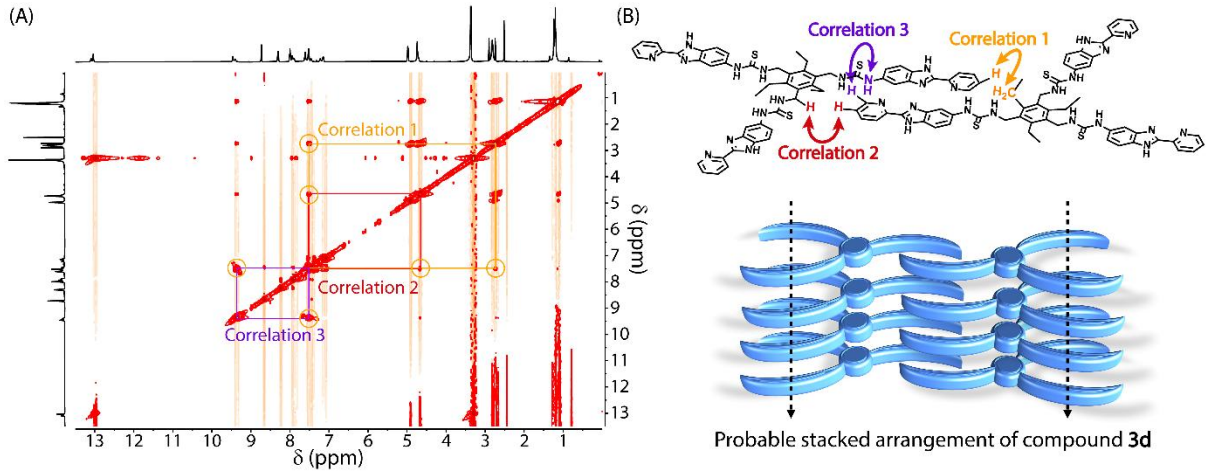

Fig. S15. NOESY spectra of compound **3d** in DMSO-d_6 solvent.

Note: To elucidate the molecular basis of the channel-forming behaviour of tripodal compound **3d**, we explored its self-assembly properties under varying solvent environments. Morphological studies revealed the formation of spherical aggregates in aqueous solution, while in chloroform, compound **3d** self-organized into nanofiber-like architectures. To investigate the origin of solvent-dependent self-assembly patterns, the 2D-NOESY NMR experiment was performed in DMSO-d_6, a solvent in which **3d** is sufficiently soluble to enable spectral acquisition. Despite the high polarity and solubilizing nature of DMSO, we observed three distinct cross-peaks, suggesting close spatial proximity between protons located on different arms, consistent with intermolecular interactions in solution. While DMSO does not fully replicate the hydrophobic environment of chloroform ($CHCl_3$) or a lipid bilayer, notable correlations between arm-to-arm interactions are still observed. This observation suggests that such interactions represent favourable contact sites even in relatively polar solvents like

DMSO. In hydrophobic environments, these interactions likely become even more dominant. As a result, they are expected to play a key role in driving the formation of the observed nanofibrous morphology. These findings collectively suggest a model in which arm-mediated intermolecular associations act as key nucleation points for higher-order organization, linking molecular self-assembly with functional channel activity.

2D-NOESY measurements also reveal proximity between the thiourea N–H protons and the pyridyl ring, supporting a preorganized geometry in which the pyridyl and benzimidazole nitrogen atoms serve as the primary ligating sites for Zn^{2+}. These correlations, however, do not provide direct evidence of S-coordination. Considering that Zn^{2+} preferentially coordinates N-donors over soft S-donors under aqueous and amphiphilic conditions, the thiourea unit is more likely to contribute indirectly by facilitating structural preorganization and cooperative self-assembly of the channel-like architecture, rather than acting as a direct S-donor during transmembrane transport. This interpretation aligns with the observed Zn^{2+} transport efficiency and provides a mechanistic rationale for the tripodal receptor's enhanced activity.

Compound **3d** is a tripodal molecule. While the canonical tripodal geometry, where ethyl groups orient outward and aromatic or functional arms point downward, is frequently observed in monomeric systems, this arrangement is not universal or fixed, and can vary depending on the environment, allowing for alternative, environment-driven self-assembly.[1, 11, 12] In this system, the experimental evidence supports such a rearrangement. The 2D-NOESY measurements of **3d** in DMSO-d_6 show strong correlations between the pyridyl aromatic proton and the thiourea N–H, as well as cross-peaks between benzylic/ethyl and pyridyl protons, consistent with intermolecular contacts that suggest two arms from separate molecules interact to stabilize a self-assembled architecture. FESEM imaging in hydrophobic media (chloroform) reveals nanowire-like aggregates, indicative of directional stacking and channel-like assembly. Taken together, these observations suggest that **3d** undergoes environment-dependent reorganization, in which two arms from each molecule engage in intermolecular interactions while the remaining arms form the channel cavity for Zn^{2+} transport. This mechanistic interpretation, illustrated in Fig. S13, provides a coherent rationale for the observed self-assembly and nanowire morphology.

6. Black lipid membrane conductance measurements:

A solvent-free black lipid membrane (BLM) was formed as previously mentioned. Briefly, a thin Teflon foil (20 μm; Goodfellow) with a 50-100 μm orifice was sandwiched between two homemade Delrin half-cells. The orifice in the Teflon foil was pre-painted with 3 μL of hexane/hexadecane on both sides, dried for 20 minutes, and filled with 2.5 mL of buffer on

each side. Before forming the lipid bilayer, about 10 µL (size of the surface around 1×1 cm^2) of a 1v% 1,2-diphytanoyl-sn-glycero-3-phosphocholine (diPhyPC) in pentane was added to the water surface. After 5-10 minutes drying, the bilayer was formed by lowering and raising the buffer level using a 5 mL pipette. The ion conductance measurements were performed with Ag-AgCl reference electrodes with a diaphragm (Metrohm, Filderstadt, Germany). One electrode (GND) was connected to ground, and the other electrode (Active) was connected to the headstage of an Axopatch 200B amplifier, which was used for conductance measurements in voltage clamp mode. Signals were filtered by an onboard low-pass Bessel filter at 1 kHz and recorded onto a computer hard drive with a sampling frequency of 2 kHz. The conductance was obtained from the averaged ion current for a series of voltage steps. All measurements were taken from at least three independent measurements. Compound **3d** (1 mM) was prepared in DMSO and diluted accordingly. To accelerate equilibrium, we added compound **6** (4 µM) on both sides of the membrane with equimolar concentrations (equilibrated for 1 h). For single-channel conductance (G) measurements, both chambers (GND and Active) were filled with a symmetrical solution containing 0.5 M $ZnCl_2$ in water. Channel formation in the presence of compound **3d** was confirmed by the distinctive channel opening and closing events after applying voltages. All data were analyzed by the ClampFit 9 software (Molecular Devices). The complete data traces were recorded over a long period, and a small portion of a large trace is presented in the manuscript and the Supporting Information (Fig. 3G and Supporting Information Fig. S14).

Calculation of ion channel diameter— The pore size is estimated from the measured single-channel pore conductance G and is proportional in first order to the bulk conductivity kappa to the pore area $S = \frac{\pi d^2}{4}$ and inversely proportional to the pore length L.

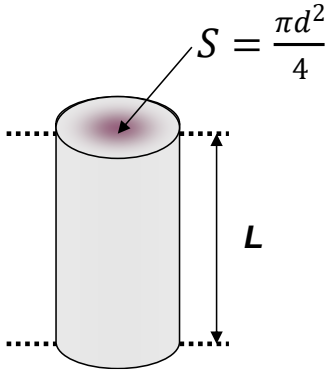

$$G = \kappa \frac{\pi d^2}{4L}; \qquad \kappa = \sum_{i=1}^{N} c_i \rho_i$$

Where our experimentally measured (from the averaged slope of the I-V plot (Fig. S15A)) conductance G = 54 pS, d = diameter of the pore, L = length of the channel = 40 Å, c_i = concentration of the ion *i,* [mol/m^3] and ρ_i = specific conductance of the ion *i*, [S·m^2/mol]. Using published values for $\rho_{Zn(II)}$ = specific conductance of the Zn^{2+} ion = 52.8 × 10^{-4} [S·m^2/mol] and $\rho_{Cl(I)}$ = specific conductance of the Cl^- ion = 76.31 ×10^{-4} [S·m^2/mol].[13] We obtained the κ = bulk conductivity = 12.9 S/m for a concentration of $ZnCl_2$ = 0.5 M. Inverting the equation yields the

pore diameter (d) = 1.5 Å. Note that the individual channels are rapidly fluctuating with short-lived larger pore radii.

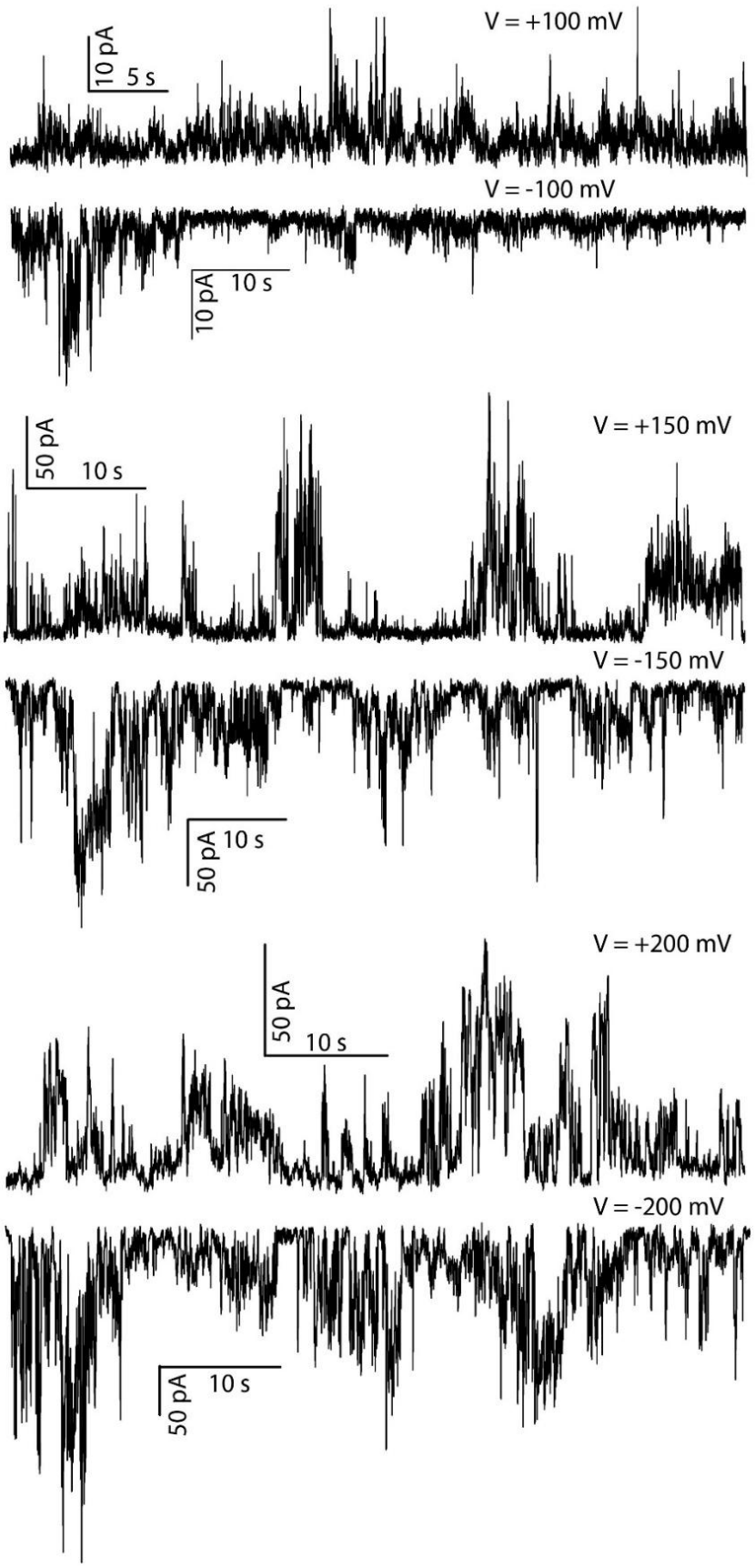

Fig. S16. Ion conductance measurements of compound **3d** (4 μM) were recorded at +100 mV, -100 mV, +150 mV, -150 mV, +200 mV, and -200 mV under symmetrical $ZnCl_2$ solutions (0.5 M).

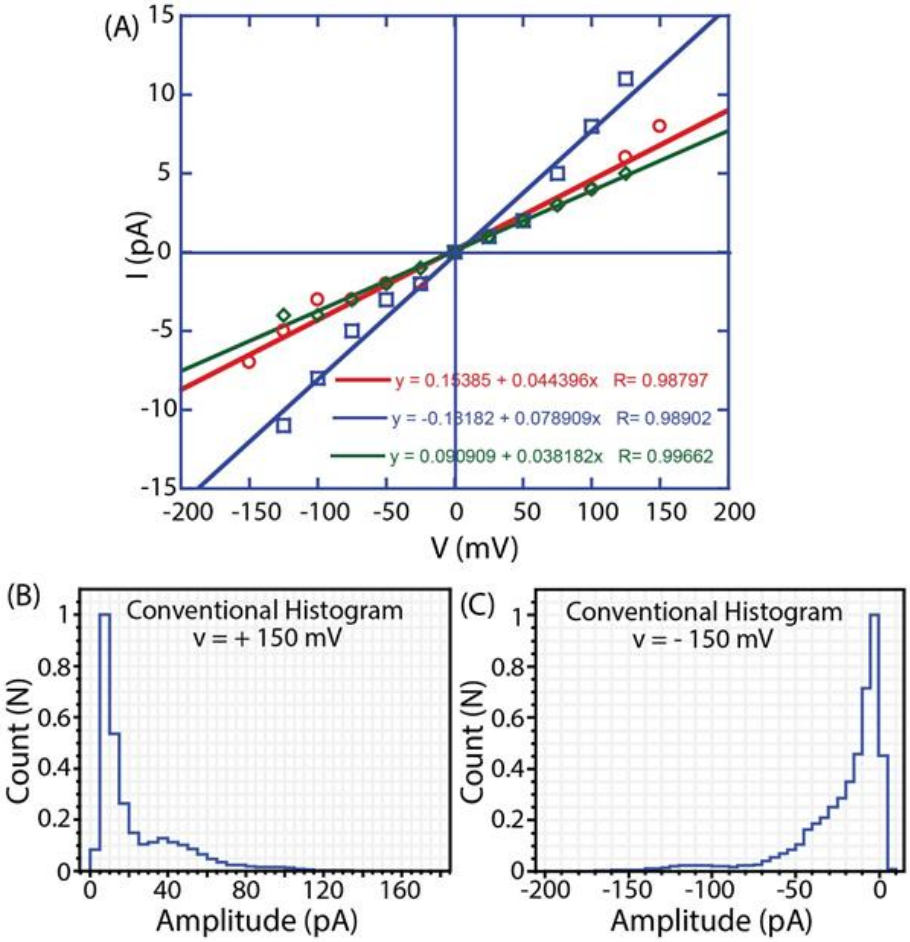

Fig. S17. (A) I–V plots of compound **3d** in symmetrical $ZnCl_2$ solution (0.5 M). This curve presents the average of a highly fluctuating ion current. Histograms of the fluctuating ion current for (B) +150 mV and (C) -150 mV in a symmetrical $ZnCl_2$ solution (0.5 M). The pronounced peak was observed at around 40 pA and 20 pA at +150 mV and -150 mV, respectively. This peak we identified as a stable single channel. Less pronounced are multiple of them.

Calculation of ions per second per channel for Zn^{2+} ion:

Conductance = 54 pS, Applied voltage = 150 mV

Current, I = Conductance × voltage = 54 pS × 150 mV = 8.1×10^{-12} A

Ions per second = $\frac{I}{ze}$ (e = 1.6×10^{-19} C) = $\frac{8.1\times10^{-12}}{2\times1.6\times10^{-19}}$ = 2.531×10^{7} ions/s

For Zn^{2+}, z =2

Therefore, the ions per second calculated for our system is 2.531×10^{7} ions/s at 150 mV.

6. ROS detection by H_2DCFDA Dye:

To evaluate reactive oxygen species (ROS) generation upon Zn^{2+}–PPIX complex, a fluorescence-based assay using 2′,7′-dichlorofluorescein diacetate (H_2DCFDA) was performed. The assay was conducted in 20 mM HEPES buffer (pH 7.0), wherein 40 µM H_2DCFDA was incubated with various combinations of 20 µM PPIX and 50 µM Zn^{2+}. Fluorescence spectra were recorded at λ_{ex} = 485 nm and λ_{em} = 522 nm. After 30 minutes of incubation, only the sample containing H_2DCFDA, PPIX, and Zn^{2+} exhibited a distinct fluorescence emission peak at 522 nm, indicating the production of ROS. No significant fluorescence was observed in the control samples. [14]

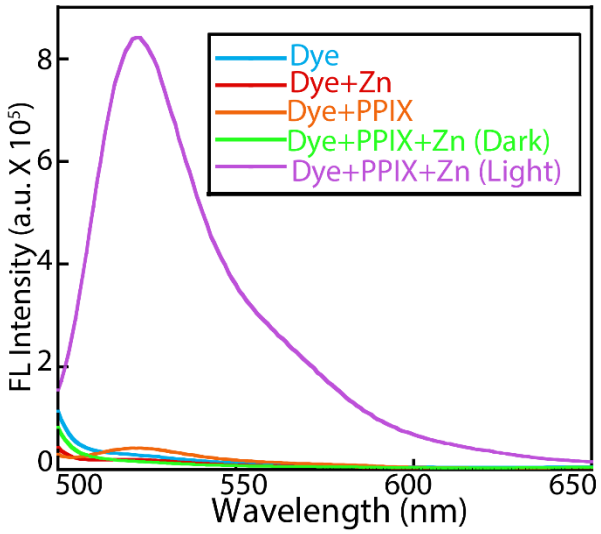

Fig. S18. ROS detection assay by H_2DCFDA dye in 20 mM HEPES buffer, pH 7.0.

7. PPIX- Zn^{2+} interaction study:

To investigate the interaction between PPIX and Zn^{2+}, both absorption and fluorescence spectroscopic analyses were conducted. Samples containing 20 µM PPIX and 50 µM Zn^{2+} were prepared in 20 mM HEPES buffer (pH 7.0). In the UV-Vis absorption spectra, a notable decrease in the Soret band at 400 nm was observed. Typically, PPIX metalation results in the reduction of the four distinct Q-bands (500–700 nm) to two peaks. However, in our measurements, all four Q-bands remained diminished yet intact, indicating that Zn^{2+} interacts with PPIX without inducing metalation. Fluorescence emission spectra were recorded with excitation at 400 nm and emission monitored at 640 nm. A marked decrease in emission intensity at 640 nm was observed in the presence of Zn^{2+}, suggesting the formation of a Zn^{2+}–PPIX complex, consistent with non-metalating binding.

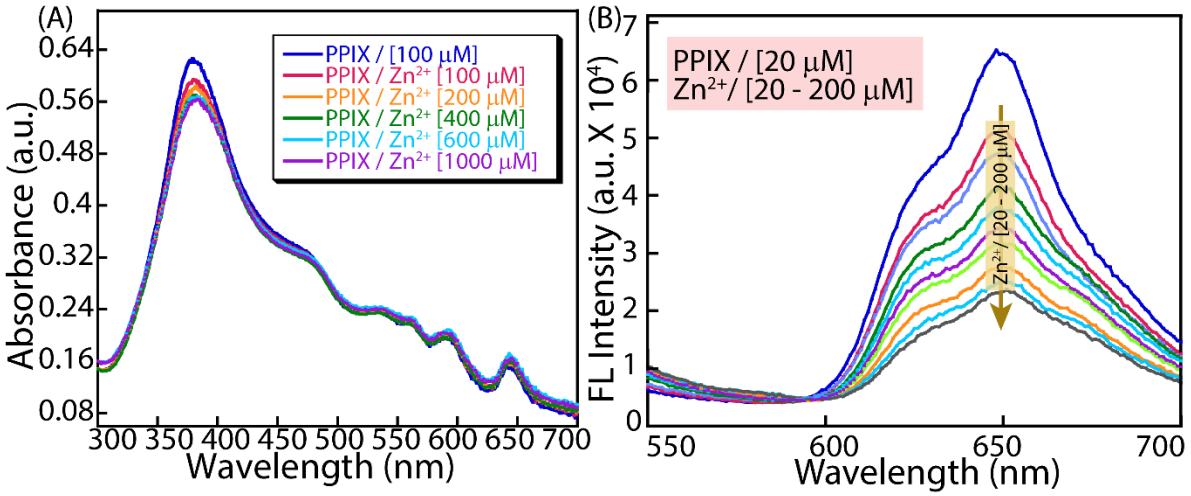

Fig. S19. (A) UV-Vis and (B) fluorescence-based PPIX and Zn^{2+} interaction studies in 20 mM HEPES buffer, pH 7.0.

Binding affinity study through UV-Vis spectrophotometer:

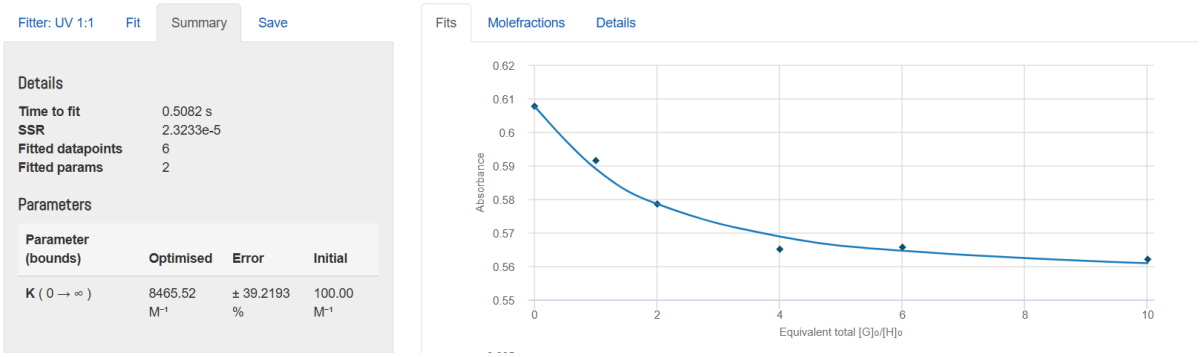

Fig. S20. Concentration-dependent variation of the Soret band of PPIX (at 400 nm) with Zn^{2+}.

The Zn^{2+} concentration-dependent (100-1000 µM) UV-Vis spectral analysis of PPIX (100 µM) was used to calculate the binding affinity using the bindfit v0.5 program. The calculated binding affinity was 8465.52 M^{-1}. This suggests that PPIX has a weak interaction with Zn^{2+}.

8. Kynurenine detection assay (Oxidation of Trp to Kyn):

We performed a UV-Vis spectrophotometric-based assay to detect the formation of kynurenine (Kyn) from tryptophan (Trp) in the presence of a PPIX-Zn^{2+} complex. The reaction mixtures contained 50 µM PPIX, 100 µM Zn^{2+}, and 1 mM Trp in 20 mM HEPES buffer (pH 7.0), combined in various permutations and exposed to white (4 h and 24 h) and red light (4 h). Following light treatment, the samples were quenched by adding 100 µL of 30% (w/v) trichloroacetic acid and then incubated at 65 °C for 30 minutes. Subsequently, 2% (w/v) p-dimethylaminobenzaldehyde (pDMAB) in acetic acid was added, and the absorbance spectra were recorded using a UV-Vis spectrophotometer. A distinct absorption peak at ~480 nm was

observed only in the sample containing all three components (PPIX, Zn^{2+}, and Trp) under light exposure, confirming the formation of Kyn. Control samples lacking one or more components, as well as the complete mixture kept in the dark, showed no significant peak at this wavelength, indicating that light exposure is crucial for the reaction to proceed.[15]

It is noteworthy that exposure to red light significantly increased kynurenine formation, whereas the same duration of white light resulted in only about 30% of the kynurenine produced under red light. Achieving a comparable level of product formation with white light required approximately 24 h.

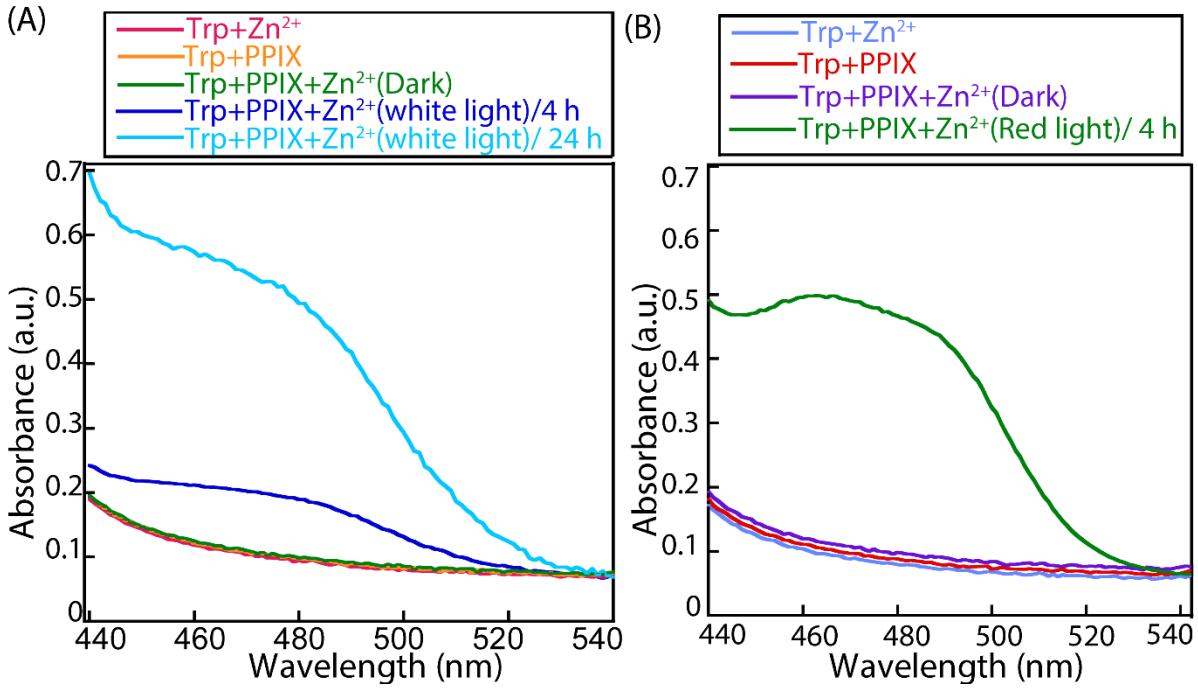

Fig. S21. UV-Vis spectral analyses for Kyn detection under varying conditions of Trp, PPIX, Zn^{2+}, with (A) visible light and (B) red light exposure.

White light contains many wavelengths, but the intensity and percentage of light overlapping Zn^{2+}-PPIX's absorption bands are relatively low, leading to weaker excitation and reduced photooxidation efficiency compared to targeted red light; additionally, white light can cause more nonspecific photodegradation of the Zn^{2+}-PPIX complex, further diminishing its effectiveness. Photodegradation was further confirmed through HPLC analysis of PPIX.

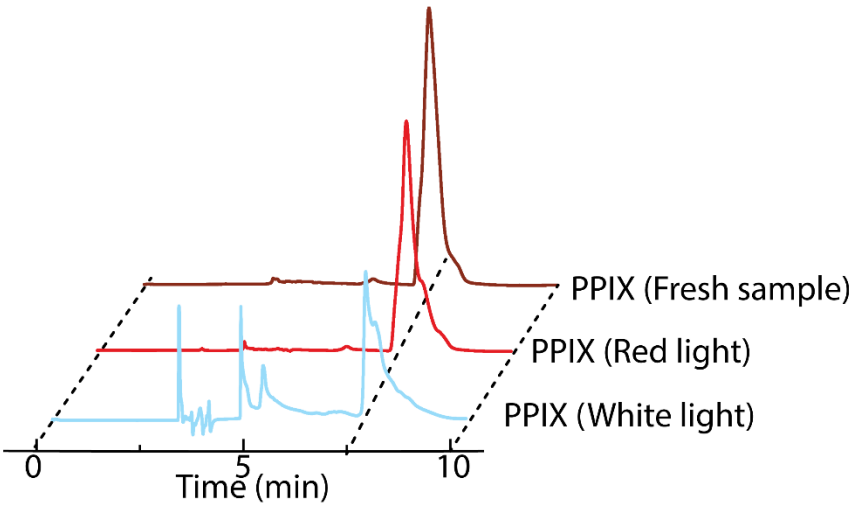

Fig. S22. HPLC analysis of PPIX photodegradation under different light exposure after 8 h.

In 20 mM HEPES buffer (pH 7.0), 50 µM PPIX was taken and exposed to white and red light for 8 h. Another fresh PPIX sample was taken as a control, and HPLC analysis of the photo-irradiated and untreated samples was conducted under similar conditions of solvent gradient as mentioned in other cases.

Note: It is noteworthy, white light consists of a broad range of wavelengths; however, only a limited portion of these overlaps with the absorption band of Zn^{2+}-PPIX. This restricted spectral overlap results in weaker excitation and diminishes photooxidation efficiency, especially compared to the selective activation provided by red light.

9. HPLC analysis for the detection of kynurenine:

The PPIX-Zn^{2+} complex-mediated Kyn formation in the presence of light was quantified using HPLC with an acetonitrile/water mobile phase system. The assay was based on monitoring the oxidation of Trp to Kyn, characteristic of indoleamine 2,3-dioxygenase 1 (IDO1) enzyme activity, by detecting absorbance at 365 nm using a UV detector. Reaction mixtures containing Trp (1 mM), protoporphyrin IX (PPIX, 20 µM), and Zn^{2+} (50 µM) were prepared in various combinations in 1 mL of 20 mM HEPES buffer (pH 7.0). Samples were exposed to red light for 4 h. Following light exposure, each sample was treated with 100 µL of 30% (w/v) trichloroacetic acid (TCA) and incubated at 65 °C for 30 minutes. The resulting mixtures were filtered through 0.2 µm PTFE syringe filters to remove particulates prior to HPLC injection. A control sample containing Trp, PPIX, and Zn^{2+} was maintained in the dark under identical conditions. For time-dependent analysis, samples containing Trp, PPIX, and Zn^{2+} were exposed to red light for 30, 60, 120, 180, and 240 minutes. Post-treatment, these samples were processed

identically for HPLC analysis. Column used: Ascentis® express C18, 2.7 µm HPLC column, flow rate: 1.0 mL/minute, mobile phase used: Optimised gradient of water/acetonitrile. The gradient used:

0-3 minutes- 20% water:80% CH_3CN

3-5 minutes- 100% CH_3CN

5-10 minutes- 20% water:80% CH_3CN

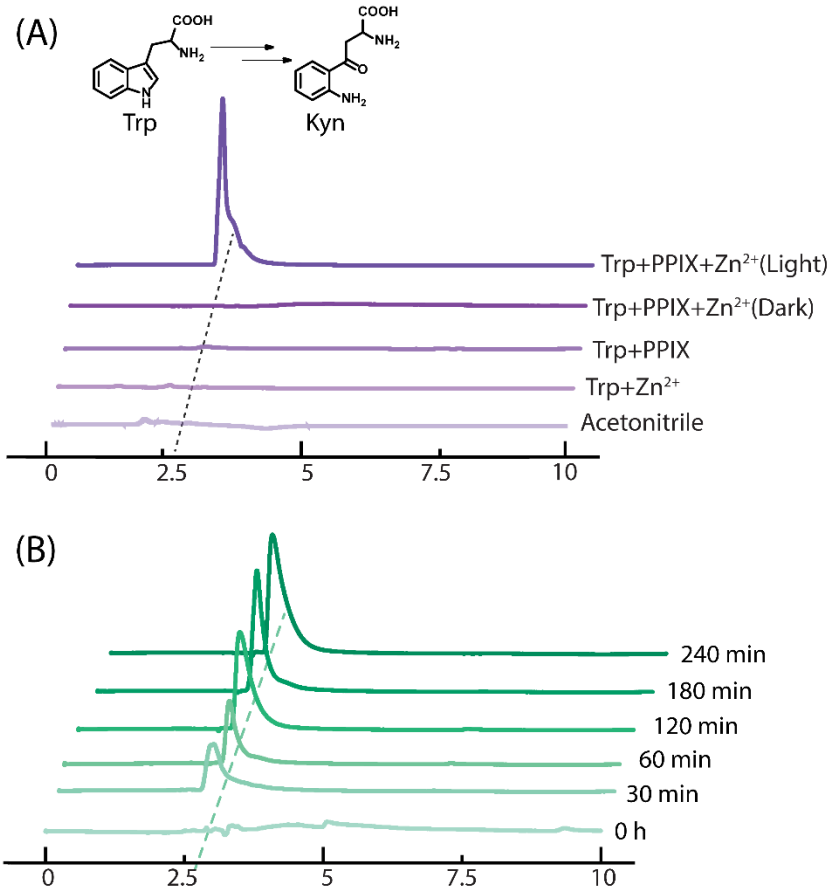

Fig. S23. (A) Control studies using HPLC for Kyn formation (different combinations of Trp, PPIX, Zn^{2+} and light). (B) Time-dependent HPLC analysis of Kyn generation from Trp (1 mM) under red light irradiation in HEPES buffer (pH 7.0) containing PPIX (20 µM) and Zn^{2+} (50 µM).

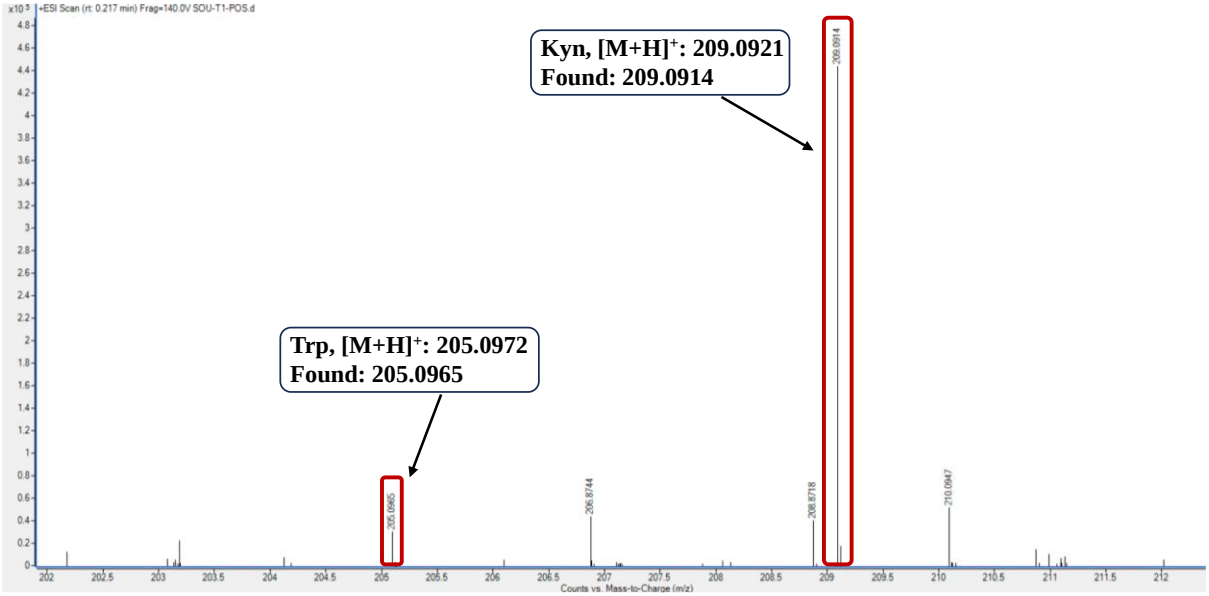

Fig. S24. HRMS analysis of Kyn generated from Trp upon photoactivation of the PPIX–Zn^{2+} complex.

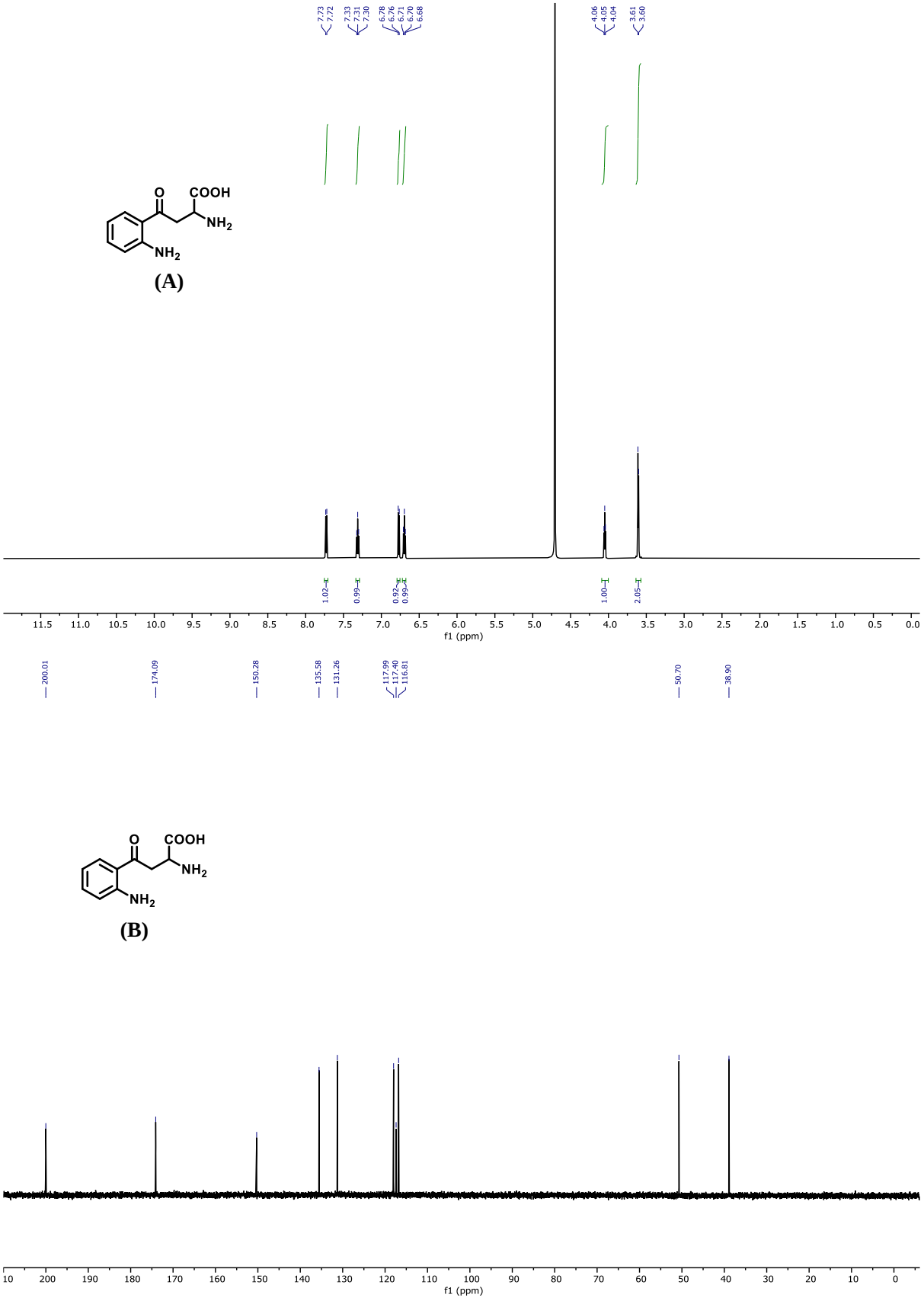

Fig. S25. (A) ^{1}H and (B) ^{13}C NMR of Kyn.

Rate of photo-oxidation of tryptophan to kynurenine:

To determine the rate of reaction, 1 mM kynurenine was treated with TCA and pDMAB according to the previous procedure, then diluted to half the original concentration to measure the absorbance at 480 nm for the 0.5 mM kynurenine pDMAB adduct, which was found to be 0.78. After 4 h of photo oxidation, the kynurenine pDMAB adduct was formed following the previous procedure, yielding an absorbance of 0.46. This was used to calculate the rate of kynurenine formation.

Product formed = $\frac{0.46}{0.78} \times 500\ \mu M = 294.87\ \mu M$

Rate of kynurenine formation = $\frac{294.87}{240}\ \mu M/minute = 1.22\ \mu M/minute$

Therefore, the rate of photo oxidation of kynurenine was 1.22 µM/minute

10. ROS scavenging analysis:

To investigate the generation of oxidative species from the PPIX-Zn^{2+} complex upon light irradiation, a ROS scavenging assay was performed using 1,4-diazabicyclo[2.2.2]octane (DABCO), ethanol[16], and catalase[17] known as $^1O_2$, hydroxyl (OH^-) and peroxide radical scavengers, respectively. Samples were prepared in 20 mM HEPES buffer (pH 7.0) containing 20 µM PPIX, 1 mM Trp, and 50 µM Zn^{2+}. To probe the role of different species of ROS, samples were supplemented with quenchers—DABCO (100 mM), ethanol (50 mM) and catalase (50 mM)—prior to irradiation. The mixtures were exposed to red-light irradiation for 4 h. Following the above-mentioned procedure, samples were prepared for Kyn detection using both UV and HPLC.

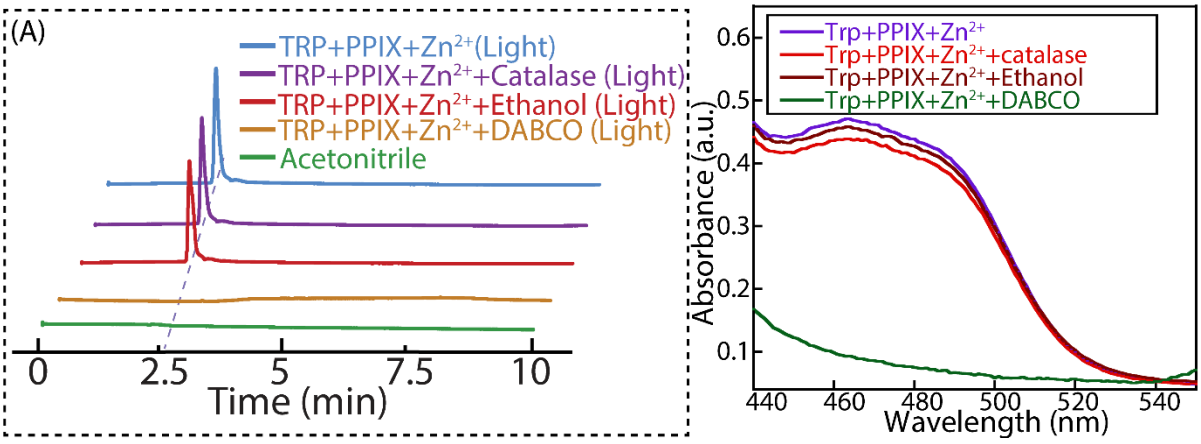

Fig. S26. Detection of Kyn in samples containing Trp, PPIX, and Zn^{2+} in 20 mM HEPES buffer (pH 7.0), treated with DABCO (100 mM), catalase (50 mM), and ethanol (50 mM) in (A) HPLC analysis and (B) UV-Vis absorbance spectra.

11. ROS-mediated oxidation reaction of different amino acids:

ROS-mediated oxidation reactions were also carried out in the presence of another substrate, such as Tyrosine (Tyr), Histidine (His), and Methionine (Met), in a 20 mM HEPES buffer, pH 7.0, under light (580-670 nm) conditions. The HRMS of the samples was recorded after 4 h of treatment for detecting the product, as represented in the following table.

Utilising the Lux meter, we have calculated the irradiance or percentage of light output:

- Calculation for red light

  6.8×10^4 lux = 1 W/ cm^2

  1360 lux (Obtained experimentally) = 0.02 W/ cm^2 = 20 mW/ cm^2
- The distance between the light source and the sample is around 5 cm.

Table S2. HRMS data detected in ROS-mediated substrate in 20 mM HEPES buffer, pH 7.0.

Substrate	**Product**	**HRMS $[M+H]^+$**	**ESI MS detected**
Tryptophan	N-formyl kynurenine	237.087	237.0905
Tyrosine	Di-tyrosine	361.1394	361.1413
Methionine	Methionine sulfoxide	166.0532	166.0530
Histidine	ND	-	-

Note: No detectable oxidation of histidine was observed under similar reaction conditions.

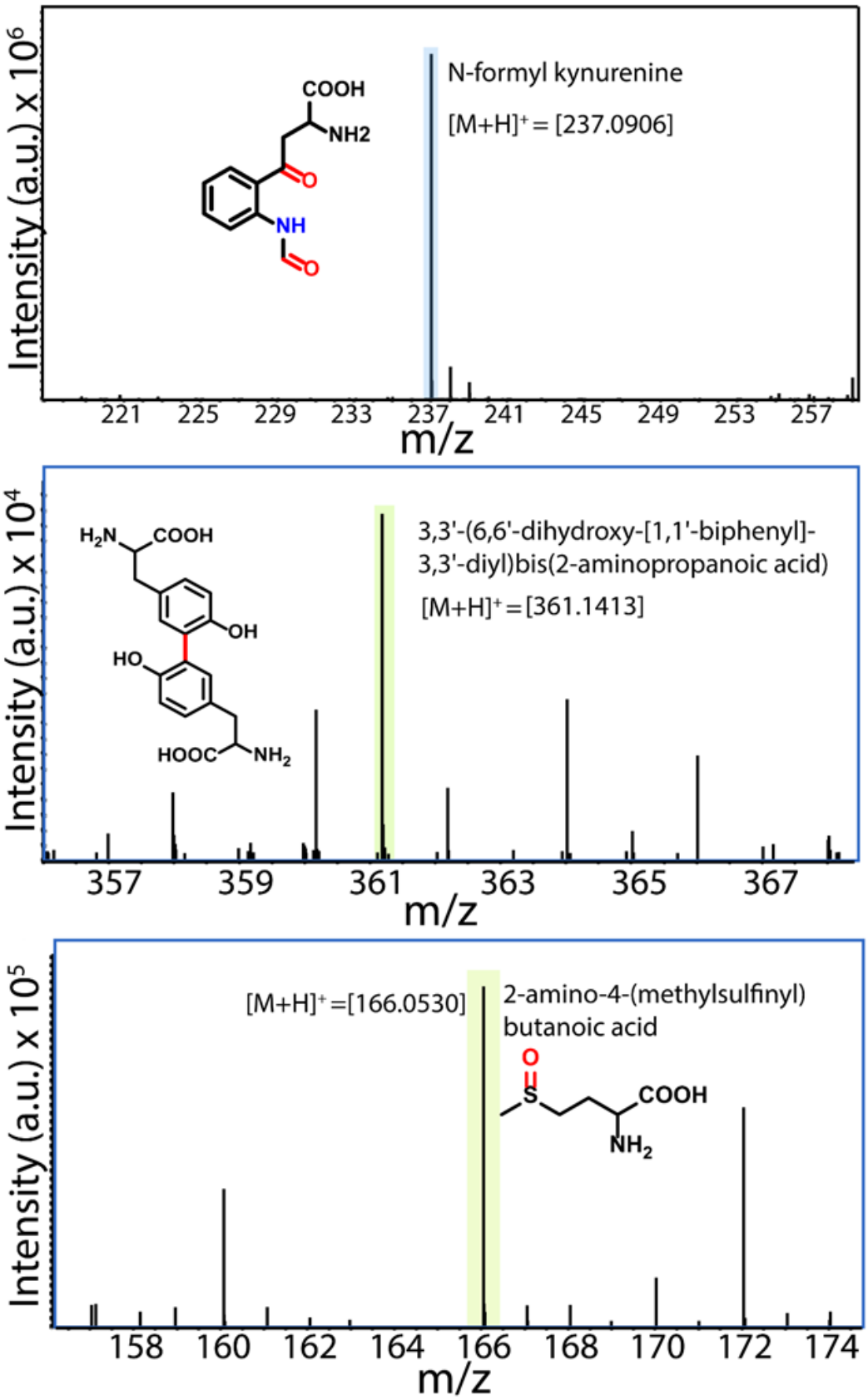

Fig. S27. HRMS spectra of the ROS-mediated reaction products.

12. HPLC analysis for the detection of kynurenine under the liposomal environment:

12.1. Preparation of EYPC/Chol-LUV⊃ PPIX/Trp − A thin lipid film was prepared by evaporating a solution of 308 µL of EYPC (50 mg/mL stock in chloroform) and 78 µL cholesterol (25 mg/mL stock in chloroform) in vacuo for 6 h. After that, the lipid film was hydrated with 1000 µL buffer (20 mM HEPES, pH 7.0) containing 100 µM PPIX, 2 mM Trp for 1 h with occasional vortexing of 4−5 times and then subjected to a freeze-thaw cycle (≥ 5 times). The vesicle solution was vortexed for 15 minutes for thorough mixing. The vesicle solution was extruded through a polycarbonate membrane with 200 nm pores 19 times (an odd number) to yield vesicles with a mean diameter of ~ 200 nm. The extracellular components, PPIX and Trp, were removed with size exclusion chromatography (Sephadex G-50) with 20 mM HEPES buffer, pH 7.0. The obtained solution was divided into 4 parts, each having 250 µL of vesicle solution (final vesicle concentration assumed: 25 mM).

12.2 Kyn detection in EYPC/Chol-LUV⊃PPIX/Trp − The obtained liposomal aliquots were treated with Zn^{2+}, compound **3d**, and red-light for 4 h in HEPES buffer pH 7.0. After photo-irradiation, the resulting vesicle solutions were lysed with 20 µL of 20% Triton X-100 and centrifuged at 10,000 rpm for 5 minutes to obtain the supernatant. The resulting solutions were filtered through 0.2 µm PTFE syringe filters to remove particulates. Further treatment was done according to the earlier section to detect Kyn in HPLC.

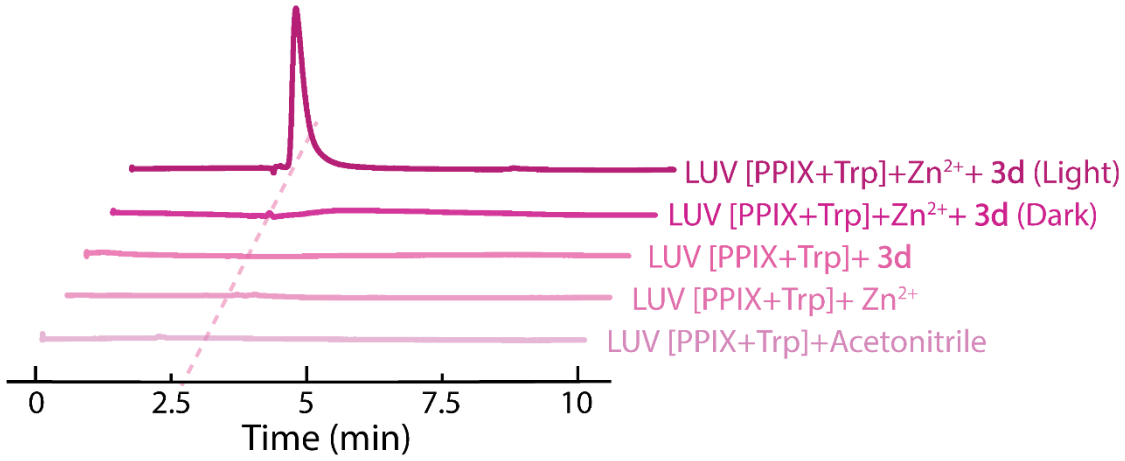

Fig. S28. HPLC analysis for kynurenine detection in EYPC/CHOL-LUVs⊃Trp/PPIX with compound **3d** and Zn^{2+} treatment.

13. Alternate light and dark treatment of EYPC/Chol-LUV⊃PPIX/Trp:

LUVs were prepared according to the earlier-mentioned procedure with a final lipid concentration of 25 mM (2 mL). Compound **3d** was equilibrated with the prepared LUV

solution, followed by the addition of Zn^{2+} ions. The resulting mixture was gently stirred and subsequently exposed to alternating red light and dark conditions for a period of 60 minutes each. At the end of every 60-minute interval, a 300 µL aliquot was withdrawn and lysed using 20 µL of 20% Triton X-100. Subsequently, these samples were analysed for Kyn using HPLC and UV Vis absorbance study as mentioned in the earlier section.

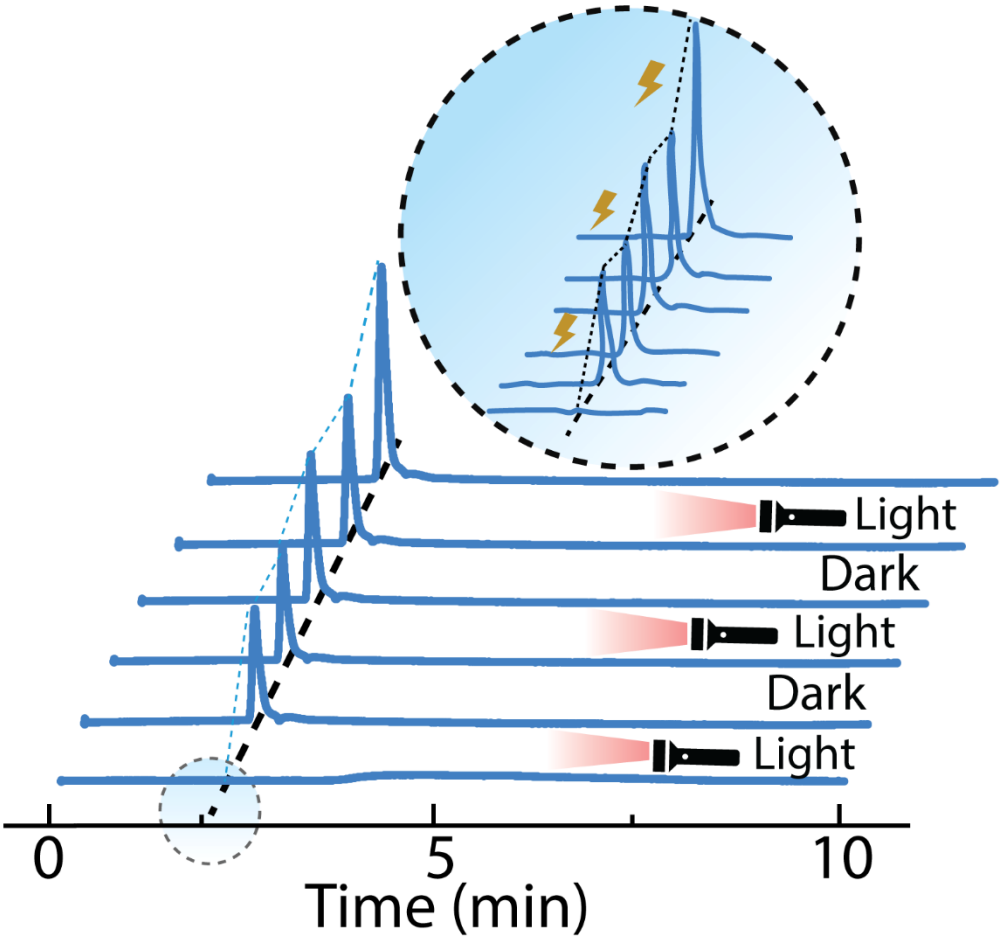

Fig. S29. HPLC analysis for Kyn detection in EYPC/Chol-LUVs⊃TRP/PPIX treated with compound **3d** and Zn^{2+} under alternate light and dark conditions at a 60-minute interval.

14. NMR spectra of the synthesized compounds:

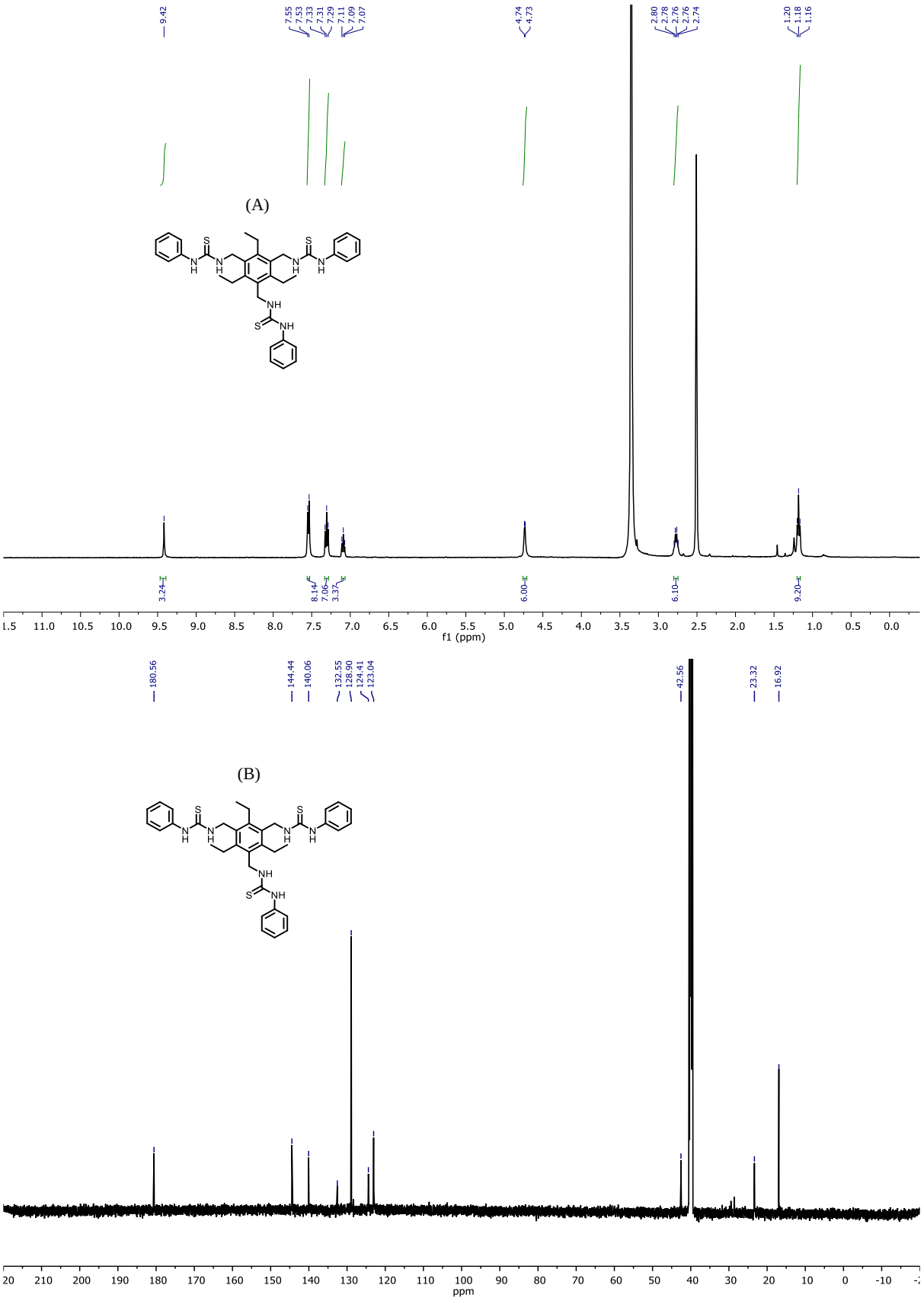

Fig. S30. ^{1}H (A) and ^{13}C NMR (B) of compound **3a** in DMSO-d_6.

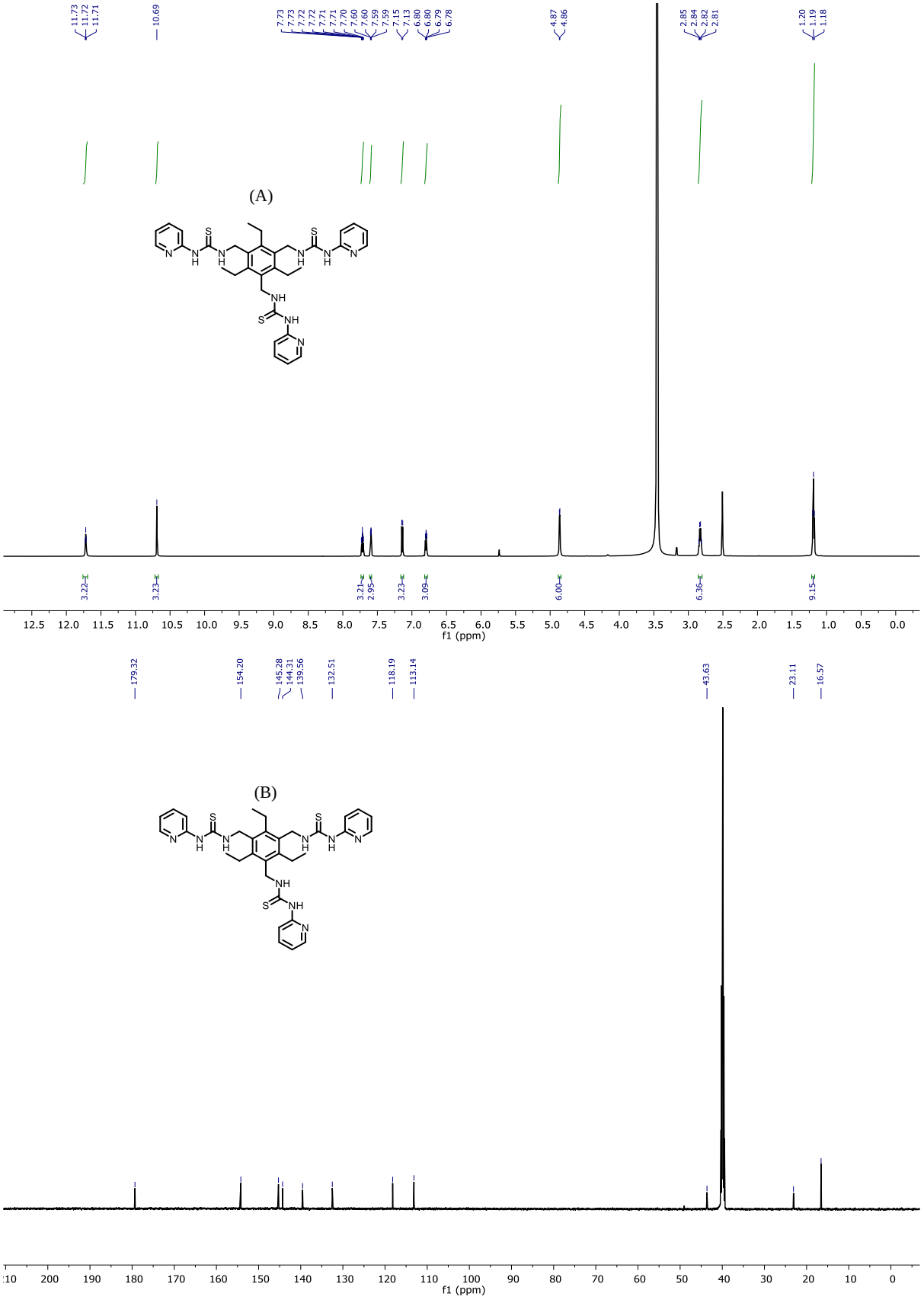

Fig. S31. ^{1}H (A) and ^{13}C NMR (B) of compound **3b** in DMSO-d_6.

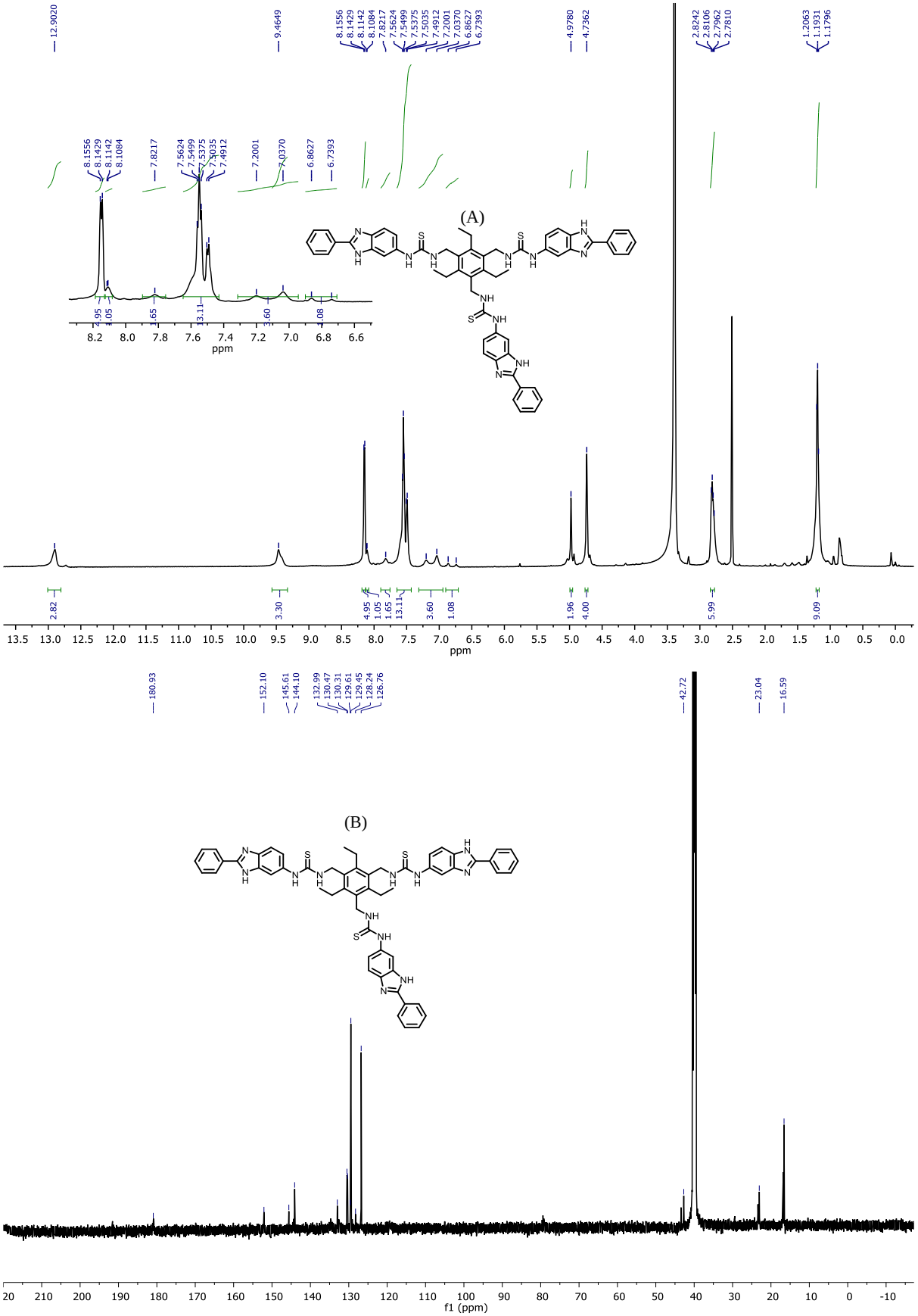

Fig. S32. ^{1}H (A) and ^{13}C NMR (B) of compound **3c** in DMSO-d_6.

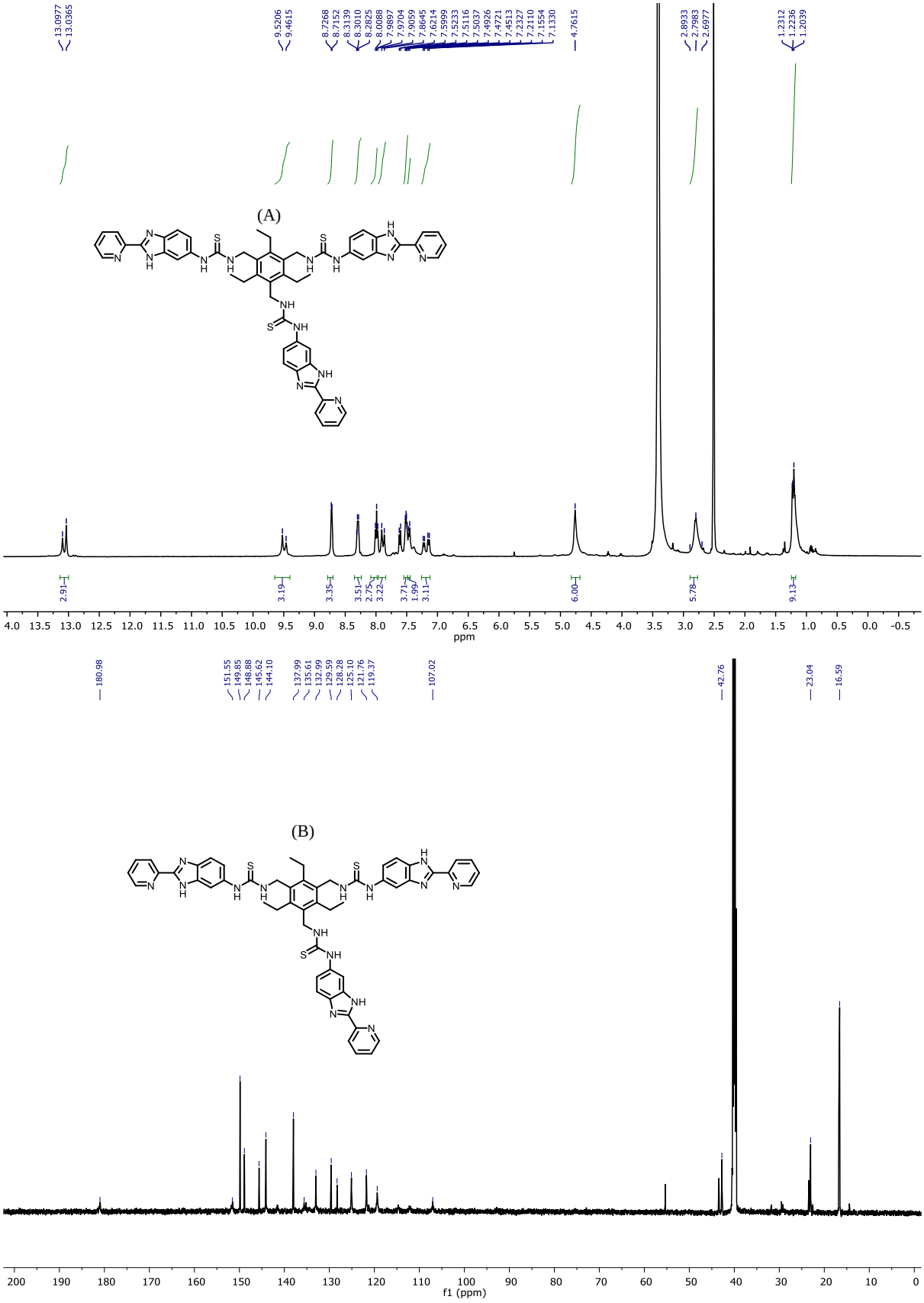

Fig. S33. ^{1}H (A) and ^{13}C NMR (B) of compound **3d** in DMSO-d_6.

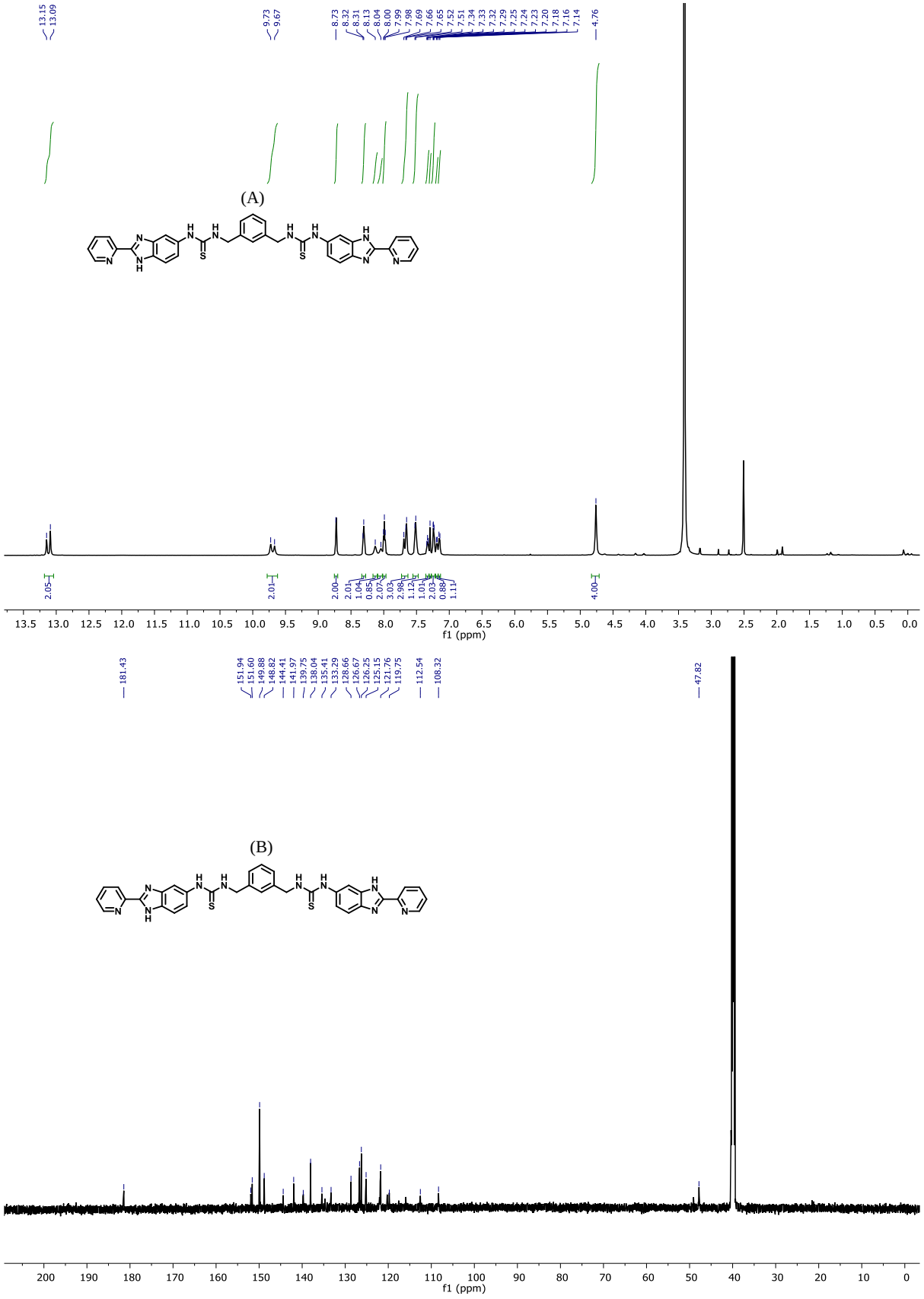

Fig. S34. ^{1}H (A) and ^{13}C NMR (B) of compound **5a** in DMSO-d_6.

References

1. N. Akhtar, N. Pradhan, A. Saha, V. Kumar, O. Biswas, S. Dey, M. Shah, S. Kumar and D. Manna, *Chem. Commun.*, 2019, **55**, 8482-8485.

2. D. A. Patrick, J. R. Gillespie, J. McQueen, M. A. Hulverson, R. M. Ranade, S. A. Creason, Z. M. Herbst, M. H. Gelb, F. S. Buckner and R. R. Tidwell, *J. Med. Chem.*, 2017, **60**, 957-971.

3. R. Schiffmann, A. Neugebauer and C. D. Klein, *J. Med. Chem.*, 2006, **49**, 511-522.

4. M. J. Langton, *Nat. Rev. Chem.*, 2021, **5**, 46-61.

5. S. A. Gartland, T. G. Johnson, E. Walkley and M. J. Langton, *Angew. Chem. Int. Ed.*, 2023, **62**, e202309080.

6. N. Akhtar, O. Biswas and D. Manna, *Chem. Commun.*, 2020, **56**, 14137-14153.

7. U. M. C. Rathnaweera, S. M. Chowdhury, R. Salam and N. Busschaert, *Chem. Rev.*, 2025, **125**, 8370-8425.

8. J. A. Malla, A. Upadhyay, P. Ghosh, D. Mondal, A. Mondal, S. Sharma and P. Talukdar, *Org. Lett.*, 2022, **24**, 4124-4128.

9. S. Chattopadhayay, A. Ghosh, T. Kumar Mukhopadhyay, R. Sharma, A. Datta and P. Talukdar, *Angew. Chem. Int. Ed.*, 2023, **62**, e202313712.

10. R. Sharma, S. Sarkar, S. Chattopadhayay, J. Mondal and P. Talukdar, *Angew. Chem. Int. Ed.*, 2024, **63**, e202319919.

11. S. J. Moore, M. Wenzel, M. E. Light, R. Morley, S. J. Bradberry, P. Gómez-Iglesias, V. Soto-Cerrato, R. Pérez-Tomás and P. A. Gale, *Chem. Sci.*, 2012, **3**, 2501-2509.

12. N. Busschaert, M. Wenzel, M. E. Light, P. Iglesias-Hernández, R. Pérez-Tomás and P. A. Gale, *J. Am. Chem. Soc.*, 2011, **133**, 14136-14148.

13. D. R. Lide, Ed., *Taylor and Francis: Boca Raton, FL*, 2007.

14. S. Dey, A. Patel, N. Haloi, S. Srimayee, S. Paul, G. K. Barik, N. Akhtar, D. Shaw, G. Hazarika and B. M. Prusty, Debasis Manna, *J. Med. Chem.*, 2023, **66**, 11078-11093.

15. N. Pradhan, N. Akhtar, B. Nath, J. Peña-García, A. Gupta, H. Pérez-Sánchez, S. Kumar and D. Manna, *Chem. Commun.*, 2021, **57**, 395-398.

16. R. Weinstain, E. N. Savariar, C. N. Felsen and R. Y. Tsien, *J. Am. Chem. Soc.*, 2014, **136**, 874-877.

17. Z. Lou, Y. Zhang, X. Liang, M. Cao, Y. Ma, P. R. Chen and X. Fan, *J. Am. Chem. Soc.*, 2025, **147**, 9716-9726.